Original Article

MOLECULAR METABOLISM

BDK inhibition acts as a catabolic switch to mimic fasting and improve metabolism in mice

Eliza Bollinger [1], Matthew Peloquin [1], Jenna Libera [1], Bina Albuquerque [1], Evanthia Pashos [1], Arun Shipstone [2], Angela Hadjipanayis [2], Zhongyuan Sun [1], Gang Xing [1], Michelle Clasquin [1], John C. Stansfield [4], Brendan Tierney [6], Steven Gernhardt [6], C. Parker Siddall [1], Timothy Greizer [1], Frank J. Geoly [3], Sarah R. Vargas [3], Lily C. Gao [1], George Williams [1], Mackenzie Marshall [1], Amy Rosado [6], Claire Steppan [6], Kevin J. Filipski [5], Bei B. Zhang [1], Russell A. Miller [1], Rachel J. Roth Flach [1,*]

ABSTRACT

Objective: Branched chain amino acid (BCAA) catabolic defects are implicated to be causal determinates of multiple diseases. This work aimed to better understand how enhancing BCAA catabolism affected metabolic homeostasis as well as the mechanisms underlying these improvements.

Methods: The rate limiting step of BCAA catabolism is the irreversible decarboxylation by the branched chain ketoacid dehydrogenase (BCKDH) enzyme complex, which is post-translationally controlled through phosphorylation by BCKDH kinase (BDK). This study utilized BT2, a small molecule allosteric inhibitor of BDK, in multiple mouse models of metabolic dysfunction and NAFLD including the high fat diet (HFD) model with acute and chronic treatment paradigms, the choline deficient and methionine minimal high fat diet (CDAHFD) model, and the low-density lipoprotein receptor null mouse model (*Ldlr*$^{-/-}$). shRNA was additionally used to knock down BDK in liver to elucidate liver-specific effects of BDK inhibition in HFD-fed mice.

Results: A rapid improvement in insulin sensitivity was observed in HFD-fed and lean mice after BT2 treatment. Resistance to steatosis was assessed in HFD-fed mice, CDAHFD-fed mice, and *Ldlr*$^{-/-}$ mice. In all cases, BT2 treatment reduced steatosis and/or inflammation. Fasting and refeeding demonstrated a lack of response to feeding-induced changes in plasma metabolites including insulin and beta-hydroxybutyrate and hepatic gene changes in BT2-treated mice. Mechanistically, BT2 treatment acutely altered the expression of genes involved in fatty acid oxidation and lipogenesis in liver, and upstream regulator analysis suggested that BT2 treatment activated PPARα. However, BT2 did not directly activate PPARα in vitro. Conversely, shRNA-AAV-mediated knockdown of BDK specifically in liver in vivo did not demonstrate any effects on glycemia, steatosis, or PPARα-mediated gene expression in mice.

Conclusions: These data suggest that BT2 treatment acutely improves metabolism and liver steatosis in multiple mouse models. While many molecular changes occur in liver in BT2-treated mice, these changes were not observed in mice with AAV-mediated shRNA knockdown of BDK. All together, these data suggest that systemic BDK inhibition is required to improve metabolism and steatosis by prolonging a fasting signature in a paracrine manner. Therefore, BCAA may act as a "fed signal" to promote nutrient storage and reduced systemic BCAA levels as shown in this study via BDK inhibition may act as a "fasting signal" to prolong the catabolic state.

Keywords BCAA; Metabolism; Metabolic syndrome; NAFLD; Diabetes

1. INTRODUCTION

Interest in branched chain amino acids (BCAAs) has intensified since untargeted metabolomic profiling identified a signature of elevated branched chain and aromatic amino acids as biomarkers of obesity & diabetes [1,2]. The initial discovery has been corroborated by numerous studies in humans and preclinical models that have demonstrated both correlative as well as causal relationships for BCAAs in diabetes development [3–6]. In recent years, defects in BCAA catabolism have also been identified in nonalcoholic fatty liver disease (NAFLD) and heart failure in humans and in preclinical models [7–13]. The BCAAs Leucine (Leu), Isoleucine (Ile) and Valine (Val) are catabolized through a conserved pathway first by the enzyme branched chain aminotransferase (BCAT) to branched chain ketoacids (BCKAs) alpha-ketoisocaproic acid (KIC/ketoleucine), 2-keto-3-methylvaleric acid (KMV/ketoisoleucine), alpha-ketoisovaleric acid (KIV/ketovaline). The BCKAs are then irreversibly catabolized by the multimeric branched chain ketoacid dehydrogenase enzyme complex (BCKDH) to downstream metabolites, which eventually enter the TCA cycle as acetyl CoA or succinyl CoA [14–16]. BCKDH is regulated at the level of

[1]Internal Medicine Research Unit, Pfizer Inc, Cambridge MA 02139, USA [2]Inflammation & Immunology Research Unit, Pfizer Inc, Cambridge MA 02139, USA [3]Drug Safety Research and Development, Pfizer Inc, Groton CT 06340, USA [4]Early Clinical Development, Pfizer Inc, Cambridge MA 02139, USA [5]Medicine Design, Pfizer Inc, Cambridge MA 02139, USA [6]Medicine Design, Pfizer Inc, Groton, CT 06340, USA

*Corresponding author. Pfizer Inc, 1 Portland St, Cambridge MA 02139, USA. E-mail: rachel.rothflach@pfizer.com (R.J. Roth Flach).

Received September 8, 2022 • Revision received October 5, 2022 • Accepted October 6, 2022 • Available online 8 October 2022

https://doi.org/10.1016/j.molmet.2022.101611

phosphorylation by branched chain ketoacid dehydrogenase kinase (BCKDK/BDK), which inhibits its activity, or by dephosphorylation via its activating phosphatase Ppm1k/Pp2cm [17,18].

Due to the strong link between BCAA elevations and cardiometabolic disease, a number of groups have sought to apply interventions such as genetic loss of function, pharmacological agents or BCAA restricted diets to understand the molecular mechanisms underlying disease-mediated elevations in BCAA, and whether these elevations are a cause or a consequence of metabolic disease [19–23]. Indeed, BCAA restriction demonstrates beneficial metabolic phenotypes in both preclinical models and humans [20,23–25]. While the phenotype of mice lacking Ppm1k has suggested that inhibition of this pathway may be causal to heart failure in preclinical models, rodents both lacking and overexpressing Ppm1k seem to display metabolic improvements [8,21,24,26]. Furthermore, animals lacking BDK have untoward developmental phenotypes such as epilepsy [27,28], thereby limiting the ability to decipher the contribution of BDK to dysregulated BCAA catabolism and metabolic disease in the model. However, in recent years, the discovery of allosteric inhibitors of BDK [29] such as BT2 [30] have allowed for modulation of BCAA catabolic activity in animals and thus investigation into the role of BCAA catabolism in metabolic disease. Indeed, BDK inhibition with BT2 increases BCAA catabolism and improves metabolic phenotypes in diabetic mice and in rats [5,21,29–31]. However, the mechanisms underlying this protection are not well understood.

Using BT2, the causal relationship between impaired BCAA catabolism and metabolic disease was assessed. Whereas previous studies treated animals for multiple weeks with BT2 [5,21], we observed that glucose tolerance and insulin sensitivity were improved acutely upon BT2 treatment. Furthermore, BT2 prevented NAFLD after treatment in multiple models including the choline deficient, methionine minimal high fat diet (CDAHFD) and the Western diet-fed low density lipoprotein receptor knockout animal (*Ldlr*$^{-/-}$), demonstrating that BDK inhibition improves metabolic disease states elicited by multiple dietary alterations and mechanisms in mice. Using a fasting/refeeding paradigm, the molecular mechanisms underlying these metabolic improvements were investigated. Interestingly, in this fast-refeed paradigm, HFD-fed animals treated with BT2 displayed an ameliorated response to feeding, which manifested as reduced postprandial insulin levels, a failure to suppress lipolysis and ketogenesis, and an absence of feeding-induced gene changes in liver as assessed by RNAseq. Further pathway evaluation demonstrated that BDK inhibition increased PPARα-mediated gene expression in liver, suggesting that signals of fasting are enhanced when BCAA catabolism is increased. These effects are likely mediated in a paracrine fashion, as liver-specific knockdown of BDK was not sufficient to modulate metabolic homeostasis, steatosis, or PPARα-mediated gene expression. Therefore, systemic BCAA levels may act as a "fed signal" to promote nutrient storage and reduced systemic BCAA levels may act as a "fasting signal" to prolong the catabolic state.

2. METHODS

2.1. Animals

All animal procedures were approved by the Pfizer Institutional Animal Care and Use Committee (IACUC). For HFD-fed mouse studies, 16-week-old male C57BL6/J mice that had been fed Research Diets 12492i for 10 weeks were purchased from Jackson laboratories and were continued on 12492i for the study duration. For CDAHFD studies, 10-week-old male C57BL6/J mice were purchased from The Jackson Laboratory and fed Purina 5053 chow or Research Diets A06071309i for the study duration. For *Ldlr*$^{-/-}$ studies, 10-week-old male *Ldlr*$^{-/-}$ mice were purchased from The Jackson Laboratory and fed Purina 5053 chow or Western diet (Research Diets D12079Bi) for the study duration. Animals were subjected to 12 h light:dark cycles. BT2 was purchased from Enamine (EN300-00845) and formulated in 5% PEG-400 (v/v)/95% of 23% hydroxypropyl beta cyclodextrin or 0.5% methylcellulose in DI water with or without 5% PEG-400 (v/v) or 1% (v/v) of Tween 80. Animals were dosed PO QD. Where indicated, animals were fasted for 16 h and refed for 2 h. For insulin injection experiments, animals were injected with 1 unit Humulin R insulin/kg (Eli Lilly). Glucose tolerance tests were performed one-hour post BT2 dose after a 16 h fast with 1 g/kg dextrose (Sigma) in water dosed orally using alpha track glucometers and strips on the dog setting.

2.2. BDK liver knockdown

AAV-U6-shBCKDK-GFP viral plasmids (SL100862) were purchased from SignaGen Laboratories. 12-week-old male C57Bl6/J mice were dosed with AAV-sh(BDK)-GFP and AAV-sh(Scramble)-GFP via retro-orbital injection at 10^{12} viral particles/mouse. Animals were put on HFD after infection.

2.3. Protein harvesting and western blot

All tissues were snap frozen in liquid nitrogen. The frozen samples were then homogenized with a hammer and approximately 50 mg was placed in 2 mL Matrix D Lysis tubes. Liver and heart samples were lysed in 800 μL Cell Signaling lysis buffer, and skeletal muscle, pancreas, and brown adipose tissue samples were lysed in 800 μL Pierce RIPA buffer. Halt protease and phosphatase inhibitors (Thermo Fisher) were added to both lysis buffers. They were lysed on the MP Fast Prep 24, according to the specific tissue settings. Samples were then spun at 12,000 RPM for 10 min and the supernatant was placed in new tubes. Total protein quantification was calculated using Pierce BCA assay for all the samples. All samples were boiled at 95 °C for 5 min with Invitrogen LDS buffer and Reducing Agent at a concentration of 2 μg/μL of total protein based on the BCA assay results. 10 μL of each sample was loaded into NuPage 4–12% Bis-Tris gels, resulting in 20 μg of protein per lane. Samples were run at 135V for 1 h and 35 min using the BioRad system. The proteins were then transferred to a PVDF membrane using the iBlot2 system. Membranes were blocked in 5% milk in TBS plus 0.05% Tween 20 for 1 h. The membranes were exposed using the Amersham 800 imager, and Imagequant software was used to analyze densitometry of each band. Primary antibodies used are detailed in the supplemental methods section.

2.4. White adipose tissue processing

Tissues were processed using a modified version of the manufacturer's protocol from the Minute™ Invent Total Protein Extraction Kit for Adipose Tissue or Cultured Adipocytes (AT-022). Halt protease and phosphatase inhibitors were added to "Buffer A" from the Invent kit. 100–200 mg of frozen tissue was added to Matrix D lysis tubes and placed on wet ice. 50 μL of Buffer A and 100 mg of the Invent kit's "protein extraction powder" were added to each tube. Samples were then homogenized on the MP Tissue Homogenizer for 60 s. An additional 50 μL of Buffer A was added to each sample, and the samples were shaken for another 30 s to 1 min. Samples were then placed in a microcentrifuge at 4 °C and spun for 2 min at 5000 RPM. The aqueous solution was then aliquoted into the Invent kit filter and collection tube, and they were then placed in the −20 °C freezer for 10 min. Following

the incubation period, the samples were spun at 5000 RPM for another 2 min at 4 °C. The filter solution was then used in a BCA assay for protein quantification.

2.5. RNA isolation

Frozen tissues were placed in Matrix D Lysis Tubes (2 mL) and homogenized in 1 mL of Qiazol and 200 μL of chloroform (Sigma). Samples were then spun for 10 min at 10,300 RPM for phase separation, and the upper aqueous phase of each sample was mixed in a 1:1 ratio with 70% ethanol. The samples were then washed in Qiagen RNEasy spin columns and reagents according to the manufacturer's protocol. Total RNA was quantified using NanoDrop. qPCR was performed using the RNA to CT one step kit (Invitrogen) according to manufacturer's instructions and the Taqman Probes (Fisher) used are listed in Supplemental Table 1.

2.6. Infusion study

Infusion studies were performed in 13-week-old DIO C57BL/6 mice on RD12492i with an indwelling jugular vein catheter (JVC) purchased from The Jackson Laboratory. Mice were acclimated and JVC lines flushed with heparin-saline solution. Prior to the study mice were fasted for 6 h, beginning at 6AM. At 10:30AM mice were connected to 2 infusion pumps, one containing a 20% solution of $^{13}C_6$-glucose (Cambridge isotopes) and infusion rate of 0.5 μL/min, and one with saline infused at 1 μL/min. Animals were free to move around their cage. One hour after the start of infusion, blood was collected from the tail for plasma, and the saline infusion line was switched with a Humulin R insulin line that was infused at a constant rate of 4 mU/kg/min. Following blood collection, animals were dosed with either vehicle or BT2 PO. Blood glucose was measured by glucometer every 5 min, and glucose was clamped to a predetermined glucose value of 250 mg/dL by increasing the glucose infusion rate. Blood was collected for plasma at 100 and 105 min following the start of the clamp period. Following the blood collection, a fluoro-deoxy-glucose FDG bolus (2 mpk) was dosed intraperitoneally, and tissues were collected from animals under isoflorane anesthesia while still being infused with glucose 10 min after receiving FDG.

2.7. Mass spectrometry

Detailed mass spectrometry methods are available in the data supplement.

2.8. RNAseq

Total RNA from 32 liver and skeletal muscle samples was evaluated for quality (RIN scores $\geq$9) by 4200 TapeStation System (Agilent, Santa Clara, CA, United States) using RNA ScreenTape (cat. 5067—5576, Agilent, Santa Clara, CA, United States). The concentrations were quantified by High Lunatic plate (cat. 7012000, Unchained Labs, Pleasanton, CA). The bulk RNASeq libraries were prepared using 400 ng of RNA with the Truseq Stranded mRNA prep kit (Illumina, 20020594) on the Perkin Elmer Janus G3 automated workstation by batching all 32 samples in one run. The final libraries were quality controlled by 4200 TapeStation System (Agilent, Santa Clara, CA, United States) using D1000 ScreenTape (cat. 5067—5582, Agilent, Santa Clara, CA, United States). The concentrations were measured using Qubit 1X dsDNA HS Assay Kit (cat. Q33231, Invitrogen- Life Technologies Corporation, Eugene, OR). The libraries were then normalized to 4 nM, re-quantitated using Qubit 1X dsDNA HS Assay Kit (cat. Q33231, Invitrogen- Life Technologies Corporation, Eugene, OR) and pooled for sequencing. The pool was loaded on NextSeq 500 sequencer for 75 Paired End run using 150 cycle High Output Sequencing Kit (cat. 20024907, Illumina, San Diego, CA). The RNAseq was analyzed using the QuickRNASeq pipeline [32]. Reads were aligned to mouse genome (mm10) using STAR (STAR version 2,5,2a) and quantified using featurecounts (version 1.5.1). Differential expression was performed using DESeq2 [33]. Data were analyzed with the use of QIAGEN IPA (QIAGEN Inc., https://digitalinsights.qiagen.com/IPA) [34].

2.9. Plasma analysis and ELISA

Whole blood samples were collected in K_2 EDTA tubes and placed on ice. Samples were then spun in a microcentrifuge at 4 °C for 10 min at 10,000 RPM. Plasma was aliquoted into separate tubes, and ALPCO Ultrasensitive Insulin ELISA (80-INSMSU-E01, E10) and Mouse/Rat FGF-21 Quantikine ELISA Kit (MF2100) and Mouse/Rat IGF-1 Quantikine ELISA Kit (791-MG) were utilized for insulin, FGF-21 and IGF-1 quantification, respectively, according to manufacturers' instructions. Other circulating plasma analytes were measured on the Siemans Advia clinical analyzer; details are listed in Supplemental Table 2.

2.10. Peroxisome Proliferator Receptor α (PPARα) coactivator assay

Using a modified version of the LanthaScreen™ TR-FRET Peroxisome Proliferator Receptor alpha Coactivator assay (Invitrogen PV4684) in agonist mode, serially diluted test compounds were spotted into 384-well black assay plates (Corning 3820) as 0.1 μL spots using an Echo acoustic dispenser (Beckman Coulter). Next, 5 μL of ice cold 2X GST-tagged PPARα ligand-binding domain (PPARα LBD) was added to the test compounds followed immediately by 5 μL mixture of 2X terbium-labeled anti-GST antibody and 2X fluorescein-labeled PGC1α coactivator peptide. Following a 1 h incubation at room temperature with shaking, the terbium emission at 495 nm and the TR-FRET signal at 520 nm were measured following excitation at 340 nm using an EnVision microplate reader (Perkin Elmer, Boston MA). Reactions were normalized to zero percent effect (ZPE) with DMSO and hundred percent effect (HPE) with 100 nM GW7647 (Tocris Bioscience). Final assay concentrations of 2.5 nM GST-tagged PPARα, 5 nM anti-GST antibody, and 250 nM PGC1α coactivator peptide were used for this assay.

2.11. *En face* aorta staining

Aortas were isolated from *Ldlr*$^{-/-}$ mice and fixed in 10% formalin overnight before transfer to PBS. Aortas were cleaned, dissected *en face*, stained with Oil red O for 5 min, and imaged with a color camera next to a microruler. Lesion area was quantified using Image J software and defined as percent stained area.

2.12. Histology, immnohistochemistry, histopathology evaluation, and digital image analysis

The pancreas, epididymal adipose tissue, and left lateral lobe of the liver was fixed in 10% formalin, embedded in paraffin, and sectioned; 5 μm sections were mounted to positively charged slides for IHC. All IHC was performed on a Leica Bond RX (Lecia Biosystems, Buffalo Grove, IL). Briefly, slides were pretreated with Epitope Retrieval Solution 1 for 20 min using heat (Lecia Biosystems, Buffalo Grove, IL). Endogenous peroxidase was quenched using a peroxidase block from the Bond Refine Polymer kit (Lecia Biosystems, Buffalo Grove, IL). Iba-1 stained slides were additionally treated with Protein Block (Agilent, Santa Clara, CA) to block non-specific binding. Iba-1(Rabbit IgG polyclonal, 1/500 or 1.0ug/ml, FUJIFILM Wako Chemicals, Richmond, VA) was incubated for 15 min at room temperature and was detected and visualized by using the Bond Refine Polymer followed by

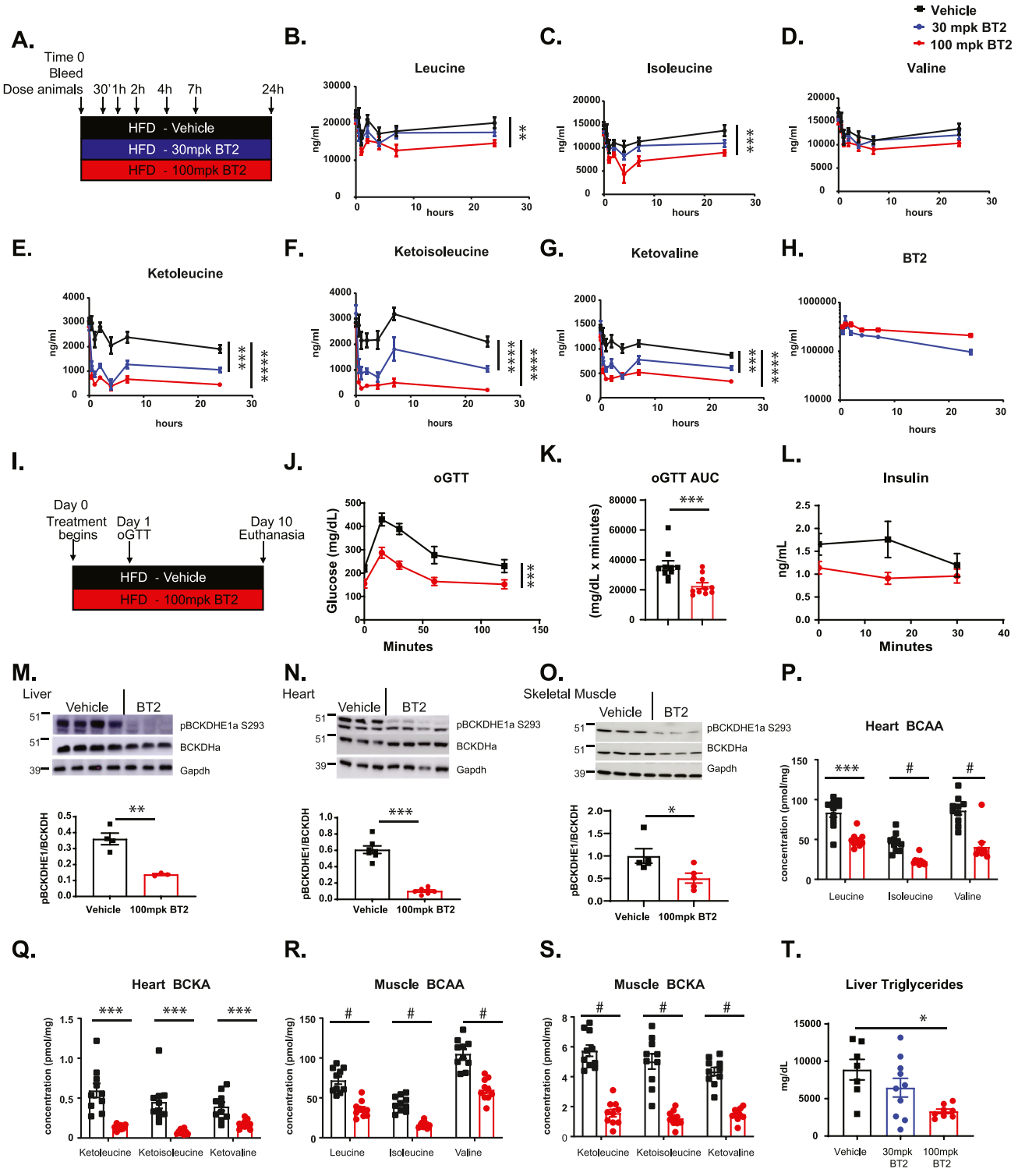

Figure 1: BT2 treatment reduces BCAA/BCKA and improves glucose tolerance and liver fat in diet-induced obese mice. A-H. Plasma BCAA/BCKA and BT2 levels after a single oral BT2 dose (30 or 100 mpk) in a time course. **A.** Study Design. **B.** Leucine, **C.** Isoleucine, **D.** Valine, **E.** Ketoleucine, **F.** Ketoisoleucine, **G.** Ketovaline, **H.** BT2. **I**–**S.** Mice were fed 60% HFD for 10 weeks, at which time, mice were dosed with 100 mpk BT2 or vehicle, fasted overnight, and dosed again. One hour later, an oral glucose tolerance test (oGTT) was performed. On day 10, the animals were euthanized. **I.** Study Design. **J.** Glucose levels during oGTT. **K.** Area under the curve (AUC) for glucose during oGTT. **L.** Insulin levels during oGTT. **M-S**. Tissues were collected 1 h post the final dose of BT2 or vehicle. **M-O.** Western blots of pBCKDHE1a, BCKDHE1a or Gapdh (**M-O**) as a loading control **M.** Liver, **N.** Heart, and **O.** Gastrocnemius muscle. Top, representative Western blot image. Bottom, densitometric analysis. **P**–**S.** BCAA/BCKA were quantified by mass spectrometry. **P-Q.** Heart, **R**–**S.** Muscle. **T.** Mice were dosed with 30 or 100 mpk BT2 or vehicle daily for 8 weeks, at which time liver TG were measured. Data represent the mean ± SEM. N = 3–12 per group; *; $p < 0.05$, **; $p < 0.01$, ***; $p < 0.005$, ****; $p < 0.0005$, #; $p < 0.0001$.

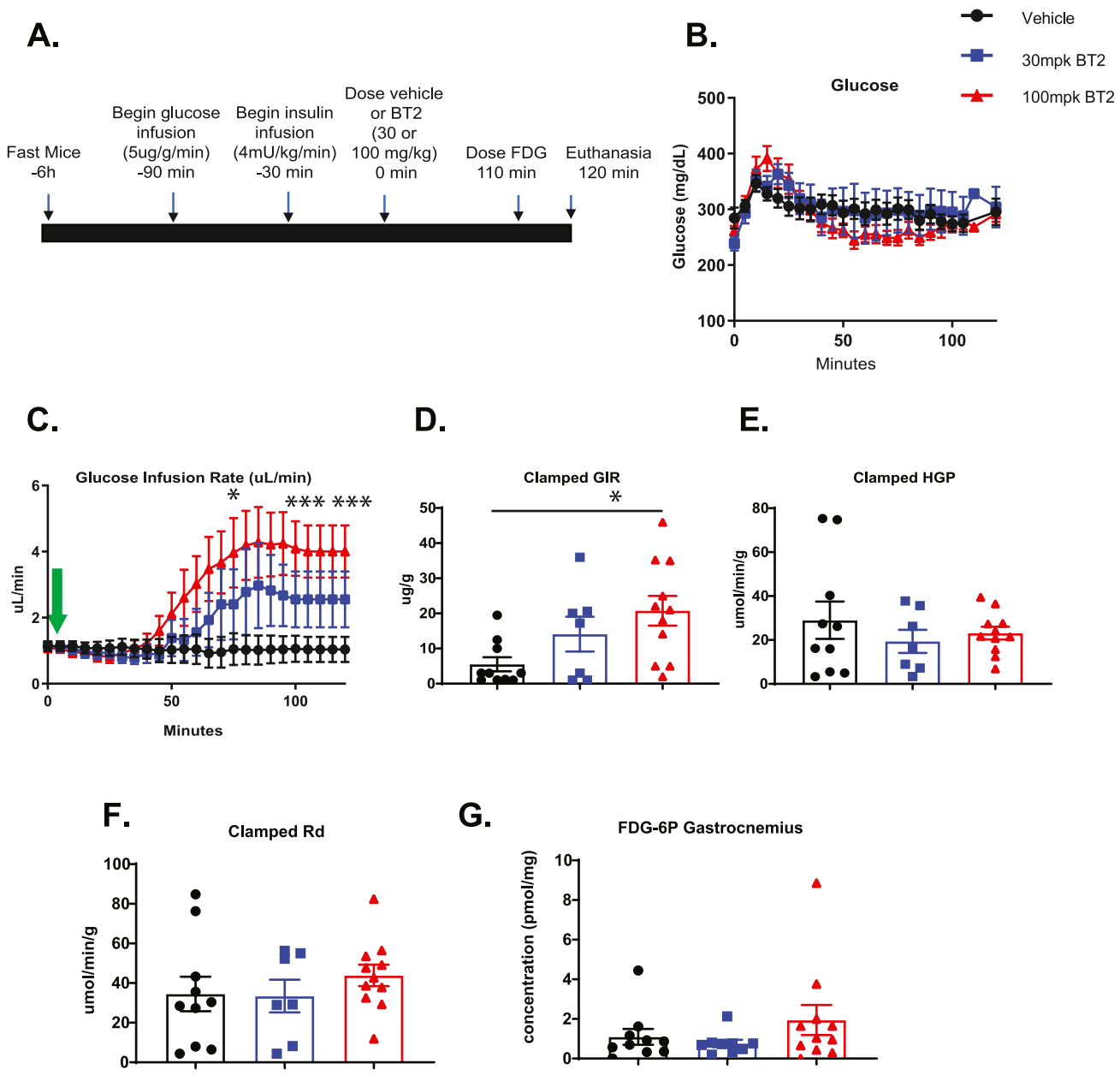

Figure 2: Acute BT2 treatment improves insulin sensitivity in diet-induced obese mice. Diet induced obese mice were implanted with a jugular vein catheter, and ^{13}C glucose was infused through one line, and insulin on a second line. Animals were dosed with vehicle or BT2 (30 & 100 mpk) at time 0. Glucose was measured via tail bleed every 5 min 10 min prior to euthanasia, FDG was injected (2 mpk). Animals were euthanized 120 min after BT2 treatment, and ^{13}C glucose ratios as well as skeletal muscle FDG levels were examined by mass spectrometry. **A.** Study design. **B.** Glycemia was maintained at 250 mg/dL throughout the study duration for all groups. **C-D.** Glucose infusion rate over the time course of the study. Arrow denotes time of compound dosing. **D.** GIR calculation. **E.** Hepatic glucose production. **F.** Clamped glucose utilization (Rd). **G.** FDG-6P in gastrocnemius muscle. Data represent the mean ± SEM. N = 7–11 per group; *; $p < 0.05$, ***; $p < 0.005$.

diaminobenzidine (DAB). Alpha smooth muscle actin (αSMA, clone 1A4 conjugated to Alexa Fluor 488, 1/500 or 0.04 μg/mL, R&D Systems, Minneapolis, MN) was incubated for 15 min followed by linker antibody rabbit anti Alexa Fluor 488 (Rabbit IgG polyclonal, 1/500 or 0.5 μg/mL, Thermo Fisher Scientific, Waltham, MA), and visualized with Bond Refine Polymer and DAB. Concentration matched isotype controls were included with each staining run: Rabbit IgG for Iba-1(1.0 μg/mL, Vector Laboratories, Burlingame, CA), and Mouse IgG2a Alexa Fluor 488 (0.04 μg/mL, R&D Systems) for αSMA. All slides were counterstained with hematoxylin, dehydrated and cleared through a series of graded alcohols and xylenes, and permanently mounted with glass coverslips. For PSR (Rowley Biochemical Inc., cat. # F-357-2, Danvers, MA), slides were deparaffinized and placed overnight in Bouin Fluid then stained using Tissue-Tek Prisma® Plus (Sakura Finetek USA Inc, Torrance, CA) as per manufacturer protocol with some optimized steps (1% Phosphomolybdic Acid for 5 min; 0.1% Sirius Red in saturated picric acid for 90 min; 2 × 30 s wash in 0.5% acetic acid). Slides were automatically dehydrated and then mounted with a permanent mounting medium. Slides were then scanned using a AT2 slide scanner for digital image analysis. A board-certified veterinary

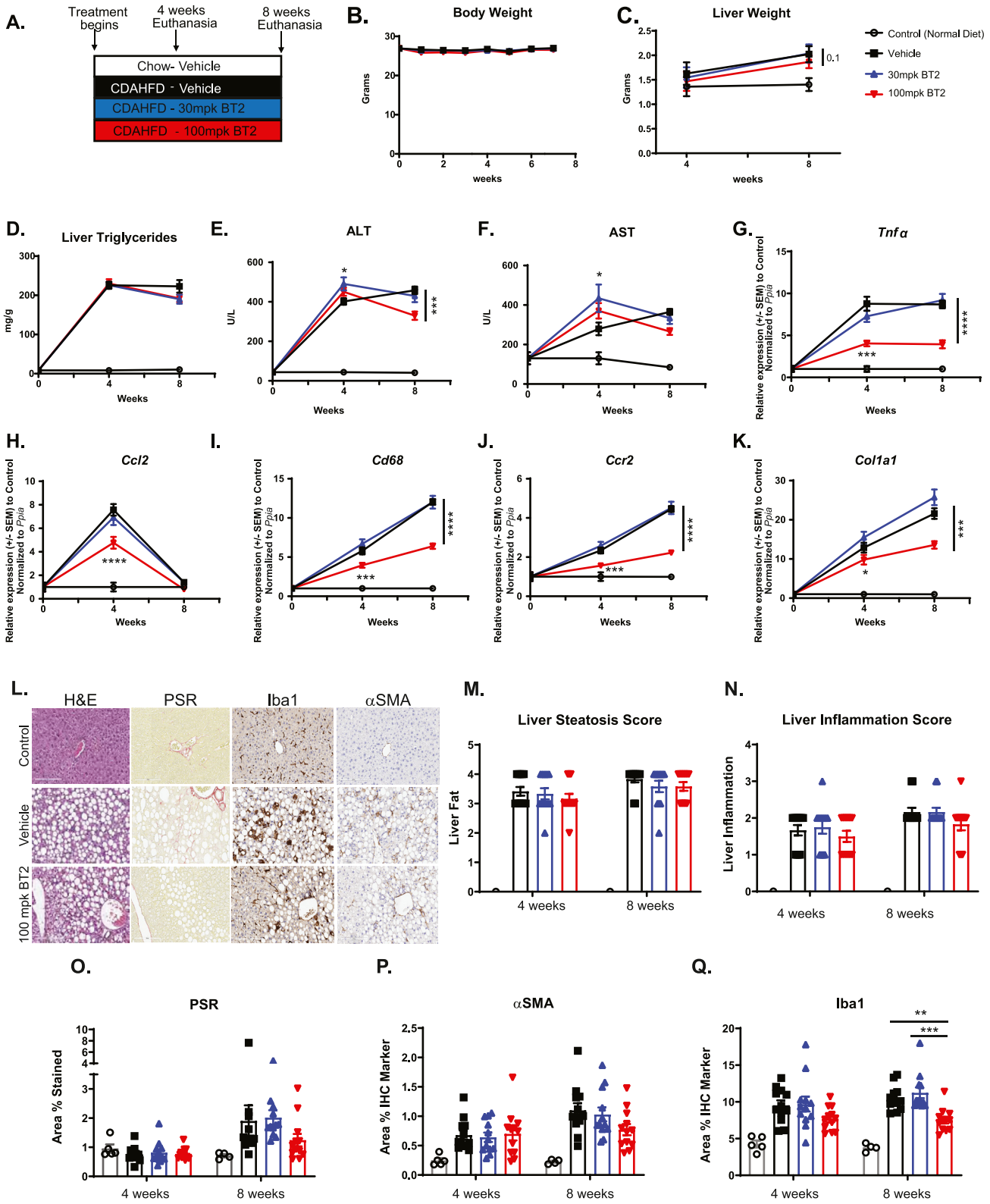

Figure 3: BT2 treatment improves liver pathology in choline deficient high fat diet. Mice were administered normal chow, or choline deficient, methionine minimal high fat diet (CDAHFD) for 8 weeks. Animals were euthanized at weeks 4 and 8 after diet administration. **A.** Study design. **B.** Body weights throughout the study duration. **C.** Liver weights. **D.** Liver triglyceride content. **E.** Plasma ALT. **F.** Plasma AST. **G-K.** RNA was extracted from liver, and quantitative RT-PCR was performed for **G.** *Tnfα*, **H.** *Ccl2*, **I.** *Cd68*, **J.** *Ccr2*, **K.** *Col1a1*. All genes were normalized to *Ppia*. **L-Q.** Representative histological sections of liver from mice fed normal chow (control), CDAHFD, or CDAHFD with 100 mpk BT2 for 8 weeks. Sections were stained as indicated. **L.** Histologic stains and IHC: From Left to Right, H&E, PSR, Iba1, α-SMA. **M-N.** Histologic qualitative grades for liver steatosis and inflammation across experimental groups. **M.** Steatosis score. **N.** Inflammation score. **O.** Quantification of PSR stain from **L. P.** Quantification of α-SMA stain from **L. Q.** Quantification of Iba1 stain from **L.** Data represent the mean ± SEM. N = 4–12 per group; *; $p < 0.05$, **; $p < 0.01$, ***; $p < 0.005$, ****; $p < 0.0005$.

pathologist who was familiar with the animal models graded H&E sections for hepatic lipid vacuolation (steatosis) and inflammation (inflammatory cell infiltrates) in a blinded fashion on a scale of 0–4. Digital image analysis was performed using Visiopharm Image Analysis Software. Tissue Finder apps were created to identify rat liver and to measure the area of the region of interest (ROI) on PSR stained slides excluding large vessels. Each image was inspected, and the region of interest was manually edited to remove artifacts or debris. Threshold parameters were applied uniformly to each image to identify and measure the positively stained area (PSR) or the area of IHC target expression (chromogen) within the liver ROI. Results were reported as percent stain (for PSR) or chromogen (for IHC) positive area within the ROI.

2.13. Statistics

A Welch's two sample t-test was performed for Figure 1J, K for the AUC, 1M–S, 7D, 8C–D (on AUC), 8E–L, S1B (on AUC), S1C–E, S1G–H, S1J–K, S5A–C. One way ANOVA was used in Figures 2E–G, 4C, 6D, S1I, S1M, S3B–C, S3E–F, S4A. A one-way ANOVA with Tukey HSD test was performed for Figure 1B–G (final timepoint), 1T, 2D, 4D, 4I, 5B, 5E–G, 5O, 5K (p4EBP), S3D, 6C, 6F (s6K), S4M. A longitudinal mixed effects model with an AR(1) covariance structure was fit in order to compare the glucose infusion rate between groups over time for Figure 2C (only data from minute 75–120 were used as this was when the trends were most linear). Longitudinal mixed effects models with an AR(1) covariance structure were fit to compare body weights between groups over time for Figures 3B, 4B, and 8B. A linear model was used for Figure 3C–K, O–Q, S2A–F. A Fisher's exact test was used for Figures 3M–N, 4F. A pairwise Wilcoxon test was performed for Figures 4G–H, 5C–D, 5I, 5K, 5M, 6B, 6F, 6H, S4B–G, S1F. All statistical analyses were performed in R 4.0.5.

3. RESULTS

3.1. Acute BT2 treatment improved glucose tolerance in diet-induced obese mice

After a single dose of BT2 treatment, there was a significant, time-dependent reduction in plasma branched chain amino acid (BCAA) and branched chain ketoacids (BCKA) that correlated with plasma BT2 exposure (Figure 1A–H). Because significant reductions in BCAA and BCKA levels were observed in mice treated with 100 mpk dose of BT2, we selected this dose for most studies to elicit maximal pharmacological effects. To understand how quickly the metabolic effects that have been previously demonstrated after BDK inhibition by the small molecule BDK inhibitor BT2 [30] could manifest, an oral glucose tolerance test (oGTT) was performed in diet-induced obese (DIO) mice after only acute treatment. Remarkably, DIO mice treated with only 2 doses of 100 mpk BT2 over 2 days showed a significant 37% improvement in glucose excursion compared to vehicle treated mice, which was accompanied by a trending reduction in insulin secretion after BT2 treatment (Figure 1I–L). In chow-fed animals, reduced glucose excursion and a trend to reduced insulin levels was also observed with BT2 treatment in the same 2-dose paradigm (Supplemental figure 1A-D). After 10 days of treatment, the tissues

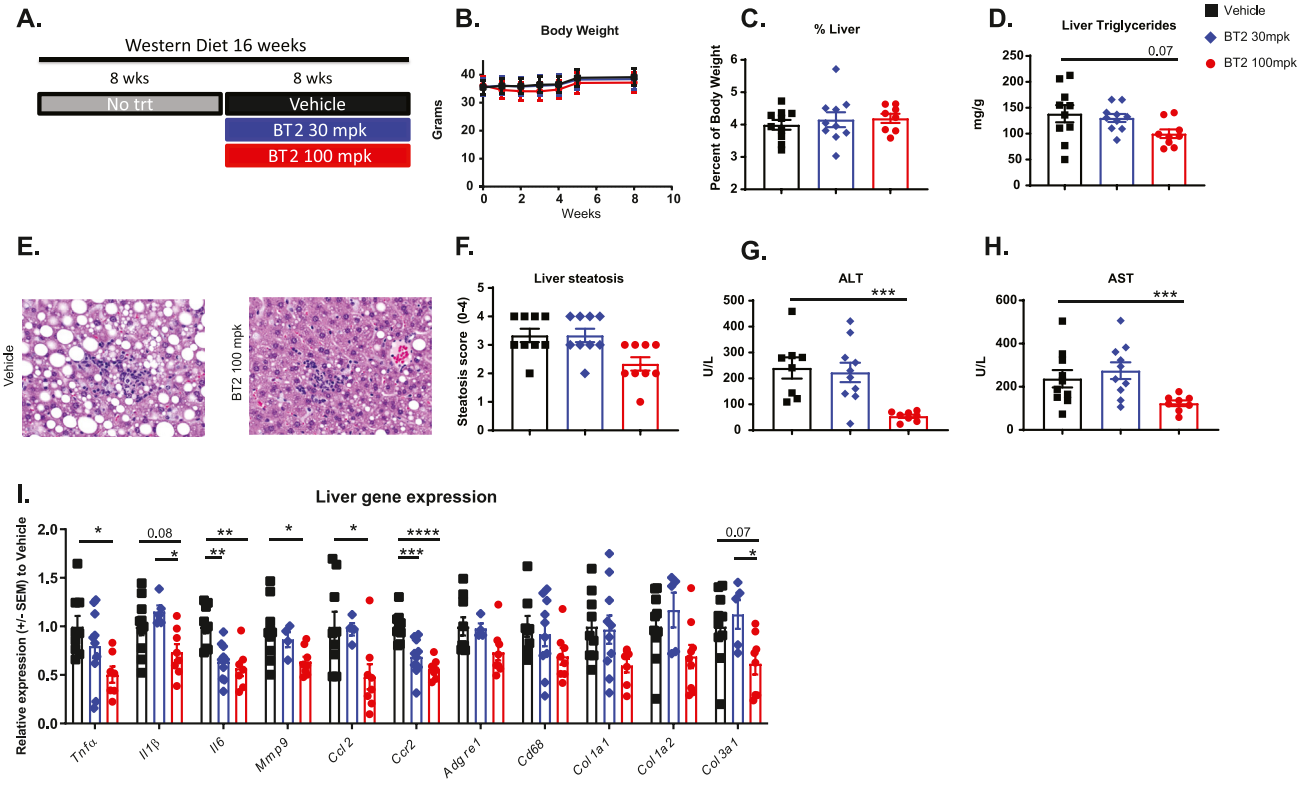

Figure 4: BT2 treatment improves liver pathology in *Ldlr*$^{-/-}$ mice fed Western diet. *Ldlr*$^{-/-}$ mice were fed Western diet for 8 weeks, at which time treatment with vehicle or BT2 was initiated and continued daily for 8 weeks. **A.** Study design. **B.** Body weight. **C.** Liver weight normalized to body weight. **D.** Liver triglyceride content. **E.** H&E-stained liver sections. Left panel (vehicle), grade 4 steatosis; right panel (100 mpk BT2), grade 1 steatosis. **F.** Qualitative grading of steatosis across experimental groups. **G.** Plasma ALT. **H.** Plasma AST. **I.** RNA was extracted from liver, and quantitative RT-PCR was performed for a number of genes and normalized to *Ppia* for input control, and vehicle treated control animals for fold change. Data represent the mean ± SEM. N = 4–10 per group; *; $p < 0.05$, **; $p < 0.01$, ***; $p < 0.005$.

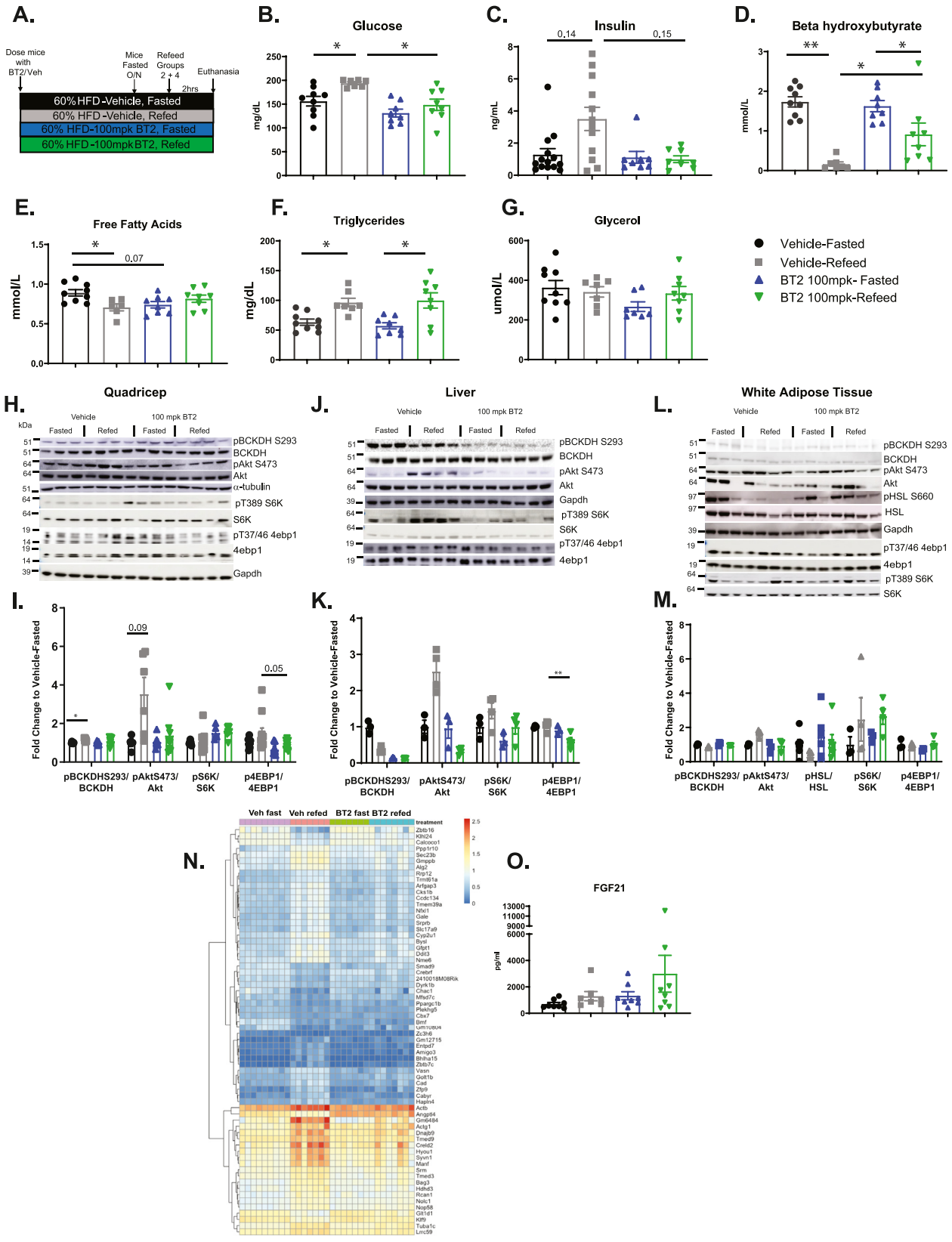

Figure 5: BT2 treatment prolongs the effects of fasting in diet-induced obese mice. Mice were treated with vehicle or BT2 in the morning, fasted overnight, dosed again with BT2 or vehicle and either remained fasting or were refed for 2 h prior to euthanasia. **A.** Study design. **B-G.** Plasma metabolites were measured. **B.** Glucose, **C.** Insulin, **D.** Beta hydroxybutyrate, **E.** Free fatty acids, **F.** Triglycerides, **G.** Glycerol. **H-M.** Protein was isolated, and Western blots were performed. **H.** Representative Western blots from skeletal muscle, **I.** Densitometric analyses of **H. J.** Representative Western blots from liver, **K.** Densitometric analysis of **J. L.** Representative Western blots from white adipose tissue (WAT), **M.** Densitometric analysis of **L. N.** RNA was extracted from liver, and RNAseq was performed. Differentially expressed genes in vehicle-treated animals after feeding are shown. This gene signature remains unchanged with BT2 treatment (N = 7–9) **O.** Plasma FGF-21 levels. Data represent the mean ± SEM. N = 3–14 per group. *; $p < 0.05$, **; $p < 0.01$.

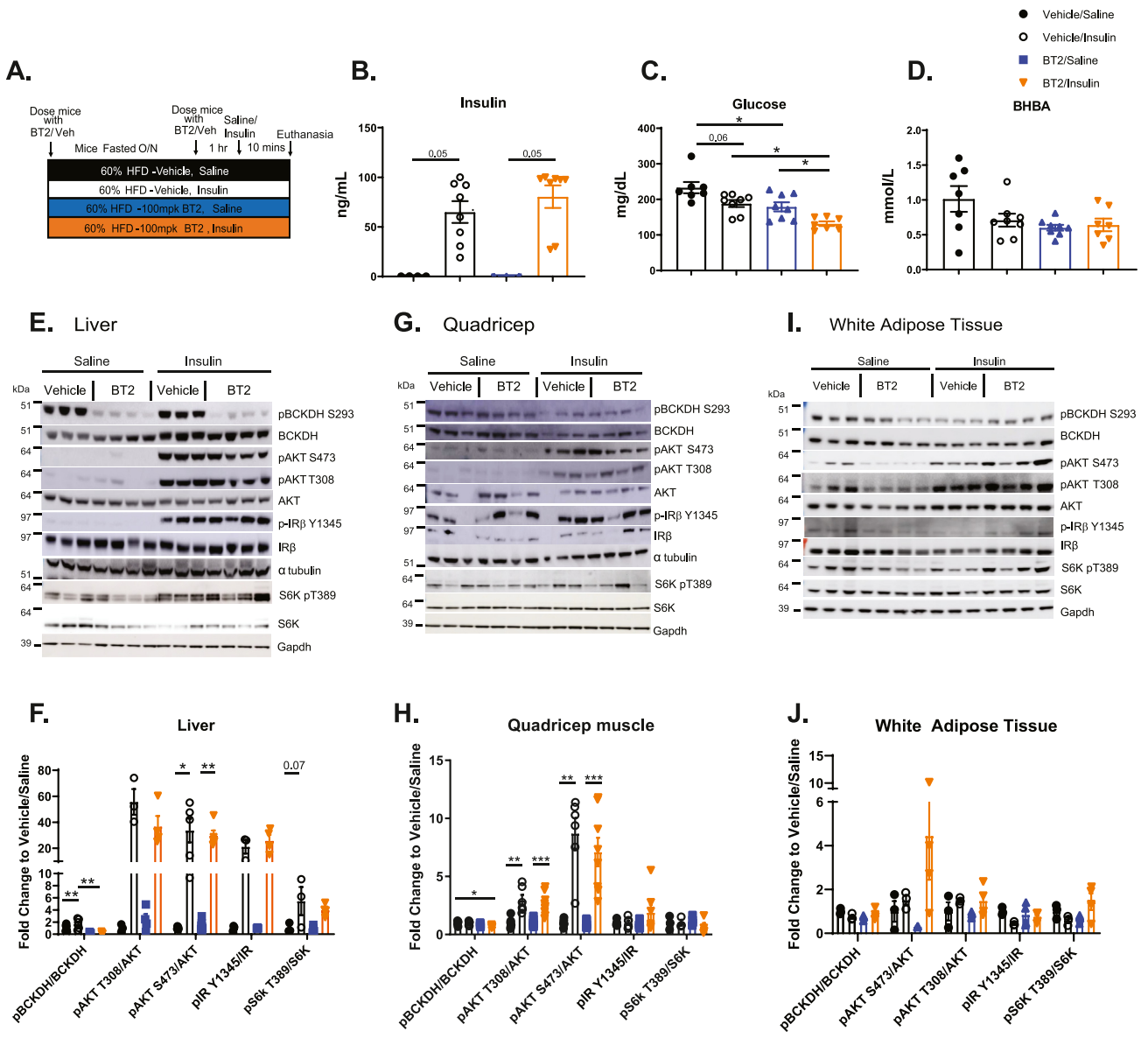

Figure 6: Insulin-mediated biochemical events and signaling are not altered in BT2-treated obese mice. Mice were treated with vehicle or BT2 in the morning, fasted overnight, dosed again with BT2 or vehicle, and 1 h later were injected with saline or insulin for 10 min, at which time animals were euthanized, and plasma and tissues were collected. **A.** Study design. **B-D.** Plasma metabolites were measured. **B.** Insulin, **C.** Glucose, **D.** Beta hydroxybutyrate. **E-H.** Protein was isolated, and Western blots were performed. **E.** Representative Western blots from Liver, **F.** Densitometric analyses of **E. G.** Representative Western blots from Quadricep muscle, **H.** Densitometric analysis of **G. I.** Representative Western blots from epididymal WAT, **J.** Densitometric analysis of **I.** Data represent the mean ± SEM. N = 3–8 per group. *; $p < 0.05$, **; $p < 0.01$, ***; $p < 0.005$.

were evaluated for changes in phosphorylation of Bckdhe1a pS293 (pBCKDH), and a significant reduction in phosphorylation was observed in the heart, liver and quadriceps muscle (Figure 1M–O). Hepatic TG were reduced with BT2 treatment, and there was a trend towards a reduced liver pathology score as measured by histological grading (Supplemental Figure 1E-F). The improvements in whole body metabolism observed could be linked to reduced mTORC1 signaling or increased AMPK signaling upon BT2 treatment. However, no significant changes were observed in downstream effectors of mTORC1 pS6k T389 and p4EBP1 T37/46, pAMPK T172 or AMPK substrate pACC S79 in the liver (Supplemental figure 1G-H). Assessment of mitochondrial markers by Western blot also demonstrated unaltered mitochondrial content in BT2-treated, HFD-fed mouse livers (Supplemental Figure 1I). Decreased plasma IGF-1 is a common fasting marker among species [35], but plasma IGF-1 levels were also not altered with BT2 treatment (Supplemental figure 1J). BT2 treatment also did not alter body weight in these animals after 10 days of treatment (Supplemental Figure 1K). Tissue extraction 1 h post final BT2 dose verified that BT2 treatment significantly reduced all BCAA and BCKA in both heart and muscle with BT2 (Figure 1P–S). A separate study in which BT2 treatment continued through 8 weeks in DIO mice was conducted. In this study, 8 weeks of BT2 treatment led to a dose-dependent significant 63% reduction in hepatic triglycerides at the 100 mpk BT2 dose level (Figure 1T), similar to previous reports [21]. There were no gross morphometric changes in epididymal WAT or pancreas tissue as assessed after H&E staining, and no significant change in overall body weight with BT2 through 7 weeks of treatment (Supplemental

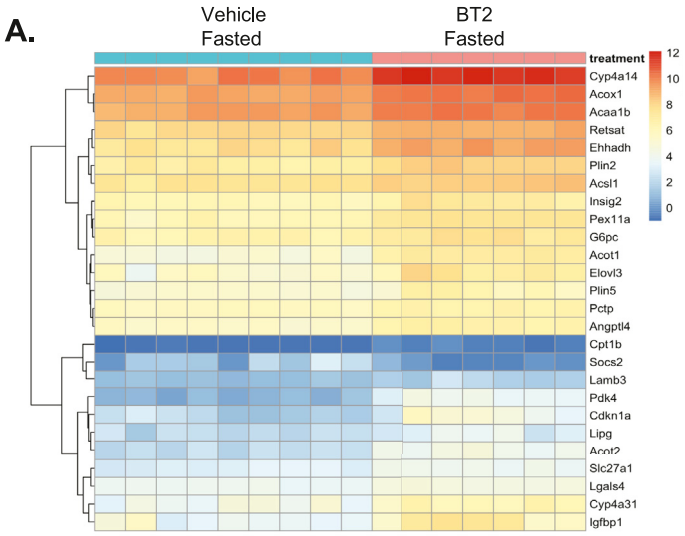

B.

BT2 fasted v Vehicle fasted

Upstream Regulator	Predicted Activation State	p-value
pirinixic acid	Activated	3.14E-20
PPARA	Activated	8.43E-19
PPARG	Activated	2.27E-16
ACOX1	Inhibited	1.56E-14
PPARD	Activated	7.02E-13
KLF15	Activated	9E-13
ciprofibrate	Activated	5.62E-12
EHHADH	Inhibited	7.48E-12
di(2-ethylhexyl) phthalate	Activated	1.2E-11
fenofibrate	Activated	1.3E-11

C.

BT2 fasted vs. Vehicle fasted

Ingenuity Canonical Pathways	-log(p-value)
Stearate Biosynthesis I (Animals)	6.11
LPS/IL-1 Mediated Inhibition of RXR Function	5.25
Mitochondrial L-carnitine Shuttle Pathway	5.22
Acyl-CoA Hydrolysis	4.1
Pregnenolone Biosynthesis	4.1
Fatty Acid β-oxidation I	4.08
Histidine Degradation VI	3.79
p53 Signaling	3.78
GADD45 Signaling	3.47
Ubiquinol-10 Biosynthesis (Eukaryotic)	3.47

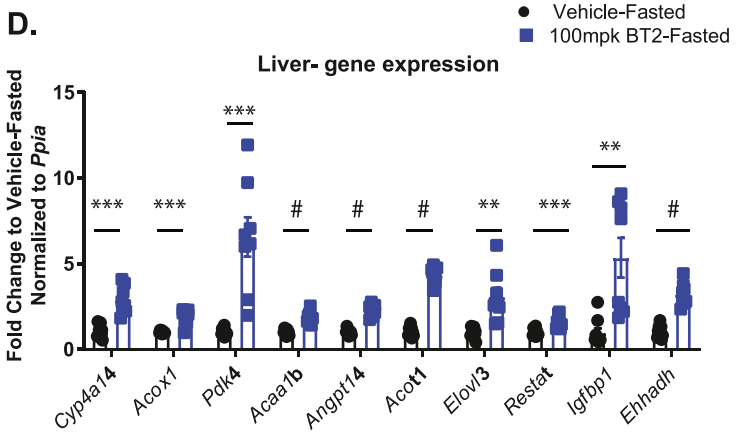

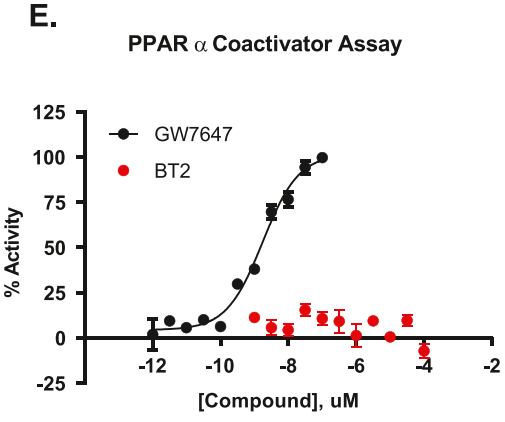

Figure 7: Indirect activation of PPARα in liver of BT2-treated mice. A-D mice were treated with BT2 or vehicle, fasted overnight, and RNAseq was performed in whole liver as described in Figure 5. **A.** Heat map of differentially expressed genes from the vehicle and BT2 treated, fasted animals. **B.** Upstream regulator analysis. **C.** Ingenuity pathway analysis. **D.** Quantitative RT-PCR was performed for a number of PPARα target genes from livers of vehicle and BT2 treated, fasted animals and normalized to *Ppia* N = 8–9 per group. **E.** PPARα coactivator Lanthascreen assay with BT2 or GW7647 as a positive control. Data represent the average of 2 independent experiments. All data represent the mean ± SEM. **; $p < 0.01$, ***; $p < 0.005$, ****; $p < 0.0005$.

Figure 1L, M). Previous studies demonstrated that BT2 treatment improved glucose handling in DIO mice and in the Zucker Fatty rat model of insulin resistance; however, that was after one week or more of treatment [5,21]. The data from this study suggest that BDK inhibition with BT2 leads to rapid improvement in glucose handling and insulin sensitivity.

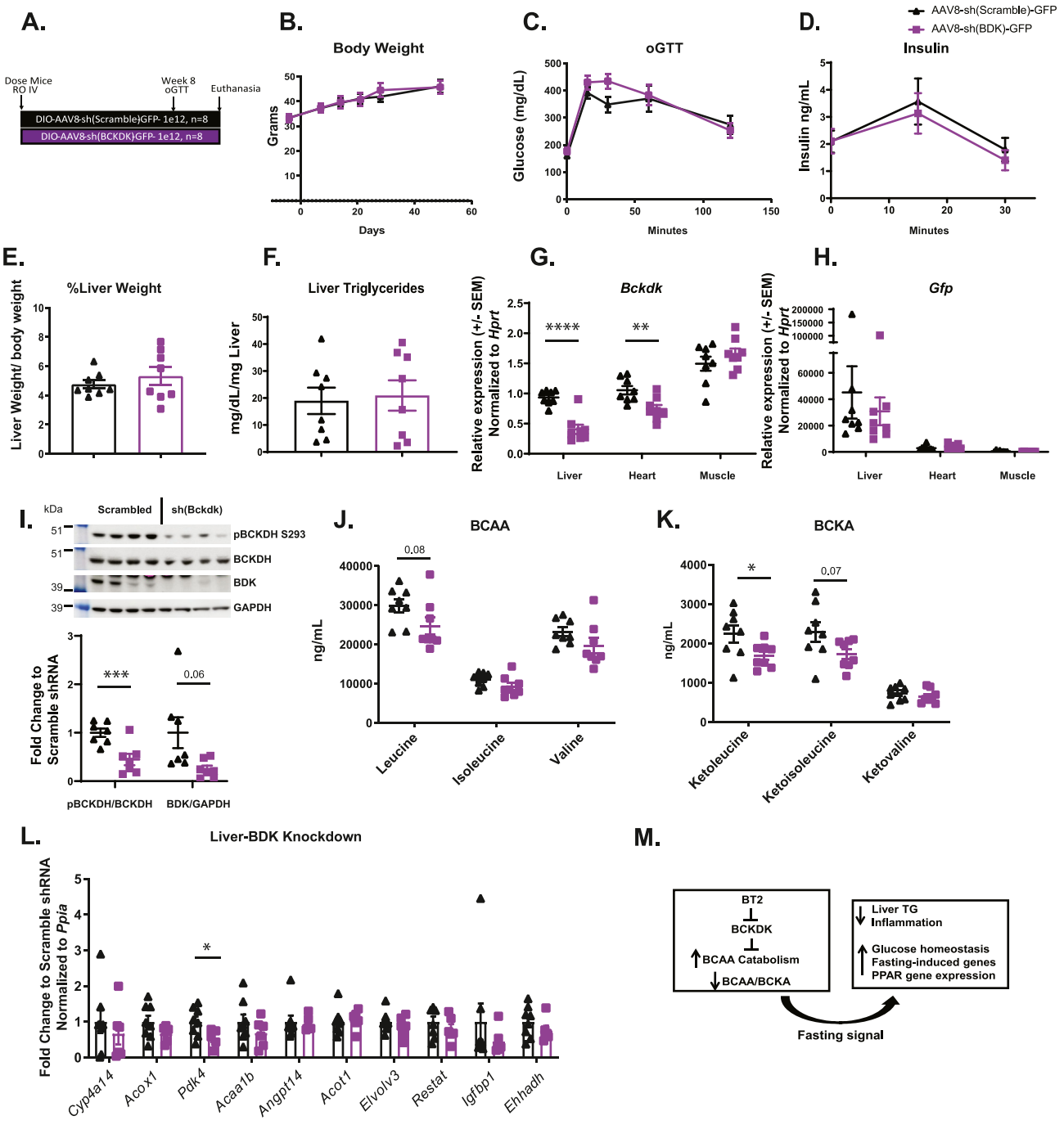

Figure 8: Liver-specific knockdown of BDK does not improve glucose tolerance or NAFLD and does not activate PPARα target genes in HFD-fed mice. BDK shRNA was injected into 12-week-old mice, and they were then put on HFD for 9 weeks. At week 8, an oral glucose tolerance test (oGTT) was performed. **A.** Study design. **B.** Body weights over the study duration. **C-D.** Oral glucose tolerance test. **C.** Glucose levels during oGTT, **D.** Insulin levels during oGTT. **E.** Liver weight as % of body weight. **F.** Liver triglycerides/mg protein. **G-H.** mRNA was isolated, and quantitative RT-PCR was performed for **G.** *Bckdk* and **H.** *Gfp* and normalized to *Hprt*. **I.** Protein was isolated, and Western blots were performed for p-Bckdh, Bckdh, Bdk, Gapdh. Top, representative images. Bottom, densitometric analyses. **J.** BCAA & **K.** BCKA were measured in terminal plasma samples. **L.** RNA was isolated from whole liver, and qPCR was performed for PPARα target genes and normalized to *Ppia*. Data represent the mean ± SEM. N = 4–8 per group. *; $p < 0.05$, **; $p < 0.01$, ****; $p < 0.0005$. **M.** Model of the mechanism underlying metabolic improvements by BT2-mediated improvements in BCAA catabolism.

3.2. Acute BT2 treatment improved acute insulin sensitivity

To understand the mechanism by which BDK inhibition with BT2 manifested a rapid improvement in insulin sensitivity, an infusion study was performed (Figure 2A). BT2 was administered acutely at low and high doses (30 and 100 mpk, respectively) in DIO mice that were infused with ^{13}C labeled glucose. Glucose levels were clamped at 250 mg/dL glucose (Figure 2B), and 15 min prior to euthanasia, fluorodeoxyglucose (FDG) was administered to measure muscle glucose uptake (Figure 2A). Interestingly, in just 45 min after BT2 administration, a dose-dependent increase in glucose infusion rate was

required to maintain plasma glucose levels, which was significant in mice treated with 100 mpk BT2 (Figure 2C, D). BCAA/BCKA are reduced by BT2 as quickly as 30 min after compound administration (Figure 1), so this timeline suggests that increased BCAA catabolism by BT2 precedes the BT2-mediated increase in GIR. There was also a non-significant 20% reduction in hepatic glucose production (Figure 2E), and a 27% increase in glucose disposal after acute treatment with 100 mpk BT2 (Figure 2F). FDG-6P was measured in gastrocnemius muscle, and a 77% increase was observed in animals treated with 100 mpk BT2 (Figure 2G); however, these changes were not statistically significant. These data suggest that upon insulin infusion, BDK inhibition with BT2 dramatically and rapidly increased insulin sensitivity, and the effects were likely mediated by a composite of multiple mechanisms such that neither glucose disposal nor hepatic glucose production alone were significantly altered by BT2 treatment.

3.3. BT2 treatment improved liver pathology in CDAHFD

Increased BCAAs have been observed in patients with NAFLD and NASH [12,36]. Previous studies demonstrated that in addition to glucose homeostasis, BDK inhibition with BT2 improved hepatic steatosis in Zucker fat rats [21], and prolonged BT2 treatment also reduced steatosis in DIO mice (Figure 1). Diets lacking methionine and choline impair hepatic lipid export and are often used to assess hepatic steatosis and hepatic inflammation. Choline-deficient, methionine minimal high fat diet (CDAHFD) can be used to induce hepatic steatosis without the weight loss observed with traditional methionine and choline deficient diets [37]. Thus, the effect of BDK inhibition in this more inflammatory NAFLD model was assessed. Mice were fed chow diet or CDAHFD and treated with vehicle or BT2 at 30 or 100 mpk PO QD for 4 or 8 weeks, and mice were euthanized at each of these time points to assess liver pathology (Figure 3A). Plasma BCAA and BCKA levels were not increased by CDAHFD, and BT2 treatment reduced all BCAA and BCKA in a dose-dependent manner (Supp. Figure 2 A–F). Body weights remained constant throughout the study duration (Figure 3B), yet liver weights increased throughout the study duration only for CDAHFD-fed mice (Figure 3C). At week 4, liver triglycerides (TGs) as well as liver enzymes alanine aminotransferase (ALT) and aspartate aminotransferase (AST) were increased in all CDAHFD-fed groups, and animals dosed with 30 mpk BT2 demonstrated higher ALT and AST than vehicle treated animals at this time point. However, by 8 weeks of CDAHFD, TG, ALT and AST levels were no longer elevated in animals dosed with 100 mpk BT2 (reduced by 14%, 28% and 27%, respectively), and the reduction in ALT was statistically significant at this dose level. These data suggest that chronic BDK inhibition may improve liver pathology in animals fed CDAHFD.

Because CDAHFD causes hepatic inflammation, inflammatory gene expression and liver inflammation were assessed by quantitative RT-PCR and immunohistochemistry in control and BT2-treated animals. Quantitative RT-PCR was performed for inflammatory cytokines *Tnfα* and *Ccl2* (Figure 3G, H), immune cell markers *Cd68*, and *Ccr2* (Figure 3I, J), and fibrotic gene *Col1a1* (Figure 3K). 100 mpk BT2 significantly reduced expression of these genes at 4- and 8-weeks diet duration compared with vehicle-treated, CDAHFD-fed animals, indicating that BT2 treatment reduced hepatic inflammatory gene expression. H&E-stained histological liver sections (Figure 3L) were evaluated by a veterinary pathologist familiar with the model but blinded to the treatment groups and scored qualitatively for hepatic lipid vacuolation (steatosis) and inflammation (inflammatory cell infiltration) on a scale of 0–4 for each feature, with score of 0 representing no microscopic pathology/normal tissue. After 8 weeks of treatment, animals treated with 100 mpk BT2 demonstrated similar steatosis scores to those treated with vehicle (Figure 3M); however, the group mean liver inflammation score was marginally lower when compared to the vehicle treated animals (Figure 3N). To quantify these changes, liver sections were stained histochemically for collagen with picrosirius red (PSR) and immunohistochemically for α-smooth muscle actin (α-SMA), a marker of activated hepatic stellate cells to quantitate fibrosis and fibrotic activity, respectively, and Iba1 (macrophage marker) to quantitate immune cell infiltration (Figure 3L) and digital image analysis performed. Correlating with the gene expression data and the qualitative histopathology, mice that had been treated with 100 mpk BT2 tended to have reduced PSR and α-SMA staining by 35% and 30%, respectively. Iba1 staining was significantly reduced in mice that had been treated with 100 mpk BT2 by 28% after 8 weeks of CDAHFD. These data suggest that chronic BDK inhibition modulates liver disease progression in this model by modulating inflammatory gene expression and lowering inflammation demonstrated histologically by lesser immune cell infiltration and collagen production/deposition.

3.4. BT2 improved liver steatosis but not atherosclerosis in *Ldlr*$^{-/-}$ mice

Hyperlipidemia, insulin resistance and inflammation can contribute to cardiometabolic diseases such as atherosclerosis. In mice, hyperlipidemic models such as *Ldlr*$^{-/-}$ must be used in the context of a high cholesterol diet to assess atherosclerosis, and these animals also develop NAFLD [38]. To assess whether BDK inhibition would improve atherosclerosis and NAFLD in *Ldlr*$^{-/-}$ mice, a reversal study was performed in which *Ldlr*$^{-/-}$ mice were fed Western diet for 8 weeks as a run-in followed by randomization by body weight and separation into three treatment groups: vehicle control or BT2 at 30 and 100 mpk PO QD for an additional 8 weeks (Figure 4A). After treatment initiation, body weights remained unchanged throughout study duration (Figure 4B). After 8 weeks of treatment, animals were euthanized. Aortas were extracted, prepared *en face*, stained with oil red O, and lesion area was quantified (Supp. Figure 3A). No differences in lesion area were observed with BT2 treatment (Supp. Figure 3B). Furthermore, while BT2 treatment significantly reduced plasma FFA levels, it did not impact plasma glucose levels, plasma TGs, or total plasma cholesterol levels in *Ldlr*$^{-/-}$ mice (Supp. Figure 3C-F). These data suggest that BDK inhibition did not improve atherosclerotic progression in this animal model.

To assess liver health, livers were extracted, weighed and processed for histology and biochemical endpoints. Liver weight as a percentage of body weight was unchanged with BT2 treatment (Figure 4C). Biochemical assessment revealed a 28% reduction in TG content in livers from *Ldlr*$^{-/-}$ mice treated with 100 mpk BT2 (Figure 4D). Target engagement was verified by Western blotting; pBCKDH was strongly reduced in liver 1 h post final dose of BT2 (Supp. Figure 2G). H&E-stained histological liver sections (Figure 4E) were evaluated by a veterinary pathologist familiar with the animal model and blinded to the treatment groups and scored qualitatively on a scale of 0–4 for hepatic lipid vacuolation (steatosis), with score of 0 representing no microscopic pathology/normal tissue. Correlating with the biochemical assessment, the mean group steatosis score tended to be lower in animals treated with 100 mpk BT2 when compared to animals receiving vehicle (Figure 4F). Interestingly, significant reductions in liver injury biomarkers ALT (79% lower than vehicle) and AST (50% lower than vehicle) were observed with 100 mpk BT2 treatment (Figure 4G, H). To assess hepatic inflammation, RNA was extracted, and qPCR was performed for a number of genes. Several inflammatory cytokines including *Tnfα*, *Il1β*, *Il6*, *Mmp9*, and *Ccl2* were significantly reduced by BT2 treatment in a dose-dependent manner (Figure 4I).

Similarly, immune cell marker *Ccr2* was significantly reduced, and *Adgre1* and *Cd68* demonstrated trends to reduction in *Ldlr*$^{-/-}$ mice treated with BT2 (Figure 4I). Finally, fibrotic genes *Col1a1* and *Col2a1* trended to reductions, and *Col3a1* was significantly reduced in liver with BT2 treatment (Figure 4I). These data suggest that BDK inhibition reduced liver inflammation and fibrotic gene expression, leading to improved liver health in this hyperlipidemic animal model.

3.5. BT2 treatment prolongs the effect of the fasting state in mice

To understand the mechanisms underlying the improvement in insulin sensitivity in mice after acute BDK inhibition, we utilized refeeding as a more physiological paradigm. DIO mice were fasted after acute treatment with 100 mpk BT2 and half were refed for 2h (Figure 5A). Animals were matched for body weight across all groups (Supp. Figure 4A). Refed, vehicle-treated mice had a 25% increase in glucose, 2.7-fold increase in insulin, 50% increase in triglycerides as well assuppression of beta-hydroxybutyrate (BHBA) and non-esterified fatty acids (FFA) in plasma, as was expected after eating (Figure 5B–E). However, after acute treatment with 100 mpk BT2, refed mice had only a 13% increase in glucose, and BHBA and FFA were suppressed to a lesser degree or were not suppressed (Figure 5B, D, E). Furthermore, BT2 treated, refed mice had no significant increase in insulin levels, which may have contributed to the lack of suppression of ketogenesis and FFA compared to vehicle-treated fasted mice (Figure 5C). These changes were accompanied by significant reductions in plasma BCAA and BCKA a trend to an increase in plasma glucagon levels, and no change in plasma IGF-1 levels in BT2-treated animals (Supp. Figure 4B-I).

pBckdh was assessed in insulin responsive tissues muscle, liver, and white adipose tissue (WAT) in response to fasting and refeeding (Figure 5H–M). While pBckdh remained unchanged in adipose tissue with refeeding, an increase in pBckdh was observed in skeletal muscle while a trend to a reduction in liver pBckdh was interestingly observed, which was further reduced with BT2 treatment (Figure 5H–M). Similar to WAT, assessment of pS293 BCKDH in both BAT and pancreas did not demonstrate significant changes upon BT2 treatment in the fasted or refed states, and there were no significant changes in pAkt induction upon BT2 treatment (Supplemental Figure 4J–M.) These data may suggest that hepatic BCAA catabolism is activated upon feeding. Refeeding tended to increase Akt pS473 as expected in vehicle treated animals in all three tissues assessed (Figure 5H–M). However, though they demonstrated acute insulin sensitivity in an infusion study (Figure 2), BT2-treated animals did not demonstrate enhanced pAkt after refeeding (Figure 5H–M). mTORC1 signaling was also assessed by immunoblotting pS6k T389, which was unchanged in muscle. However, in liver, there tended to be reduced pS6k upon fasting and refeeding in BT2 treated animals. In WAT there tended to be increased pS6k upon BT2 treatment. p4EBP1 was not significantly altered with BT2 treatment in WAT but was reduced after refeeding in muscle and livers of BT2-treated animals (Figure 5H–M). Phosphorylation of hormone sensitive lipase (pHSL), a regulator of lipolysis, was reduced after re-feeding in vehicle treated mouse WAT, it remained elevated in BT2-treated mouse WAT (Figure 5L–M), suggesting that these animals were not responding to the refeeding.

Livers were isolated, and RNAseq was performed in vehicle- and BT2-treated fasted and refed groups (Figure 5N). In the fasted state, most genes associated with BCAA catabolism were not significantly changed in liver by BT2 treatment, although *Bcat2* was downregulated and *Klf15* trended towards an increase (Supplemental Figure 5A). Using a threshold of 1.25-fold change and 10% false discovery rate (FDR), 431 genes were differentially expressed in the vehicle fasted vs. the vehicle refeed group. Interestingly, comparison of the BT2 fasted group and the BT2 refed groups using these same criteria found no significant gene expression differences (subset of genes shown in Figure 5N). These data suggested that the liver remained in a state of fasting-associated gene expression after BT2 treatment. Hormones such as FGF21 may be induced upon prolonged fasting [39], and indeed, while not significant, FGF21 levels were 89% increased in BT2-treated animals compared with those that had been treated with vehicle (Figure 5O). In summary, these data suggest that BDK inhibition maintains a metabolically fasted state including prolonged fasting-induced gene expression and physiology. RNAseq was additionally performed in gastrocnemius muscle in the same animals upon fasting and refeeding, but when the same analysis was applied (1.25 FC and 10% FDR), no significant gene expression changes were observed upon acute BT2 treatment (Supplemental Figure 5B). However, *Klf15* and *Bcat2* were slightly, yet significantly, upregulated. Quantitative RT-PCR was also performed for genes involved with BCAA catabolism in WAT upon acute BT2 treatment, and no significant changes were observed (Supplemental Figure 5C).

The lack of pAkt induction (Figure 5) yet improvements in insulin sensitivity (Figure 2), in BT2-treated animals seemed paradoxical. We postulated that the lack of pAkt induction could have been due to the lack of insulin elevation in BT2-treated animals and not due to reduced insulin sensitivity (Figure 5C). To test this hypothesis, 4 groups of DIO animals were administered BT2 or vehicle, fasted overnight, and then injected with saline or an insulin bolus for 10 min prior to euthanasia, and 1 h after treatment (Figure 6A). Acute increases in circulating insulin were observed post-injection, as expected (Figure 6B). Concomitantly, reduced glucose and BHBA levels were observed in vehicle-treated mice, while BT2-treated animals displayed baseline reductions in these values (Figure 6B–D). Liver, muscle, and WAT were extracted and immunoblotted for pBckdh, pS473 and pT308 Akt, pT389 s6K as well as p-IRβ to assess insulin signaling mechanics in response to an insulin bolus. Similar inductions in pAkt/Akt at both pS473 and pT308 sites, pT389 s6K and pIR/IR were observed in both vehicle- and BT2-treated animal groups in muscle and liver (Figure 6E–H). However, in WAT, pS473 induction tended to be increased after BT2 treatment but this was not a statistically significant result (Figure 6I, J). These data suggest that BDK inhibition with BT2 does not ameliorate the biochemical responses of many of the key signaling components induced by an insulin bolus in mice and suggests that many of the phenotypes observed in the refed condition could have been due to a lack of glucose elevation or insulin induction after refeeding (Figure 5C).

3.6. Acute BT2 treatment alters PPARα target gene expression

In addition to comparing the gene expression changes in fasted and refed animals, the differences in gene expression in fasted vehicle or fasted BT2-treated animals was assessed. Using a 1.25-fold change cutoff and FDR of 0.1, there were 180 differentially expressed genes in BT2-and vehicle-fasted mouse livers (subset shown in Figure 7A). Upstream regulator analysis identified several candidate pathways that could be responsible for the differentially expressed gene signature observed including Peroxisome proliferator activated receptors alpha, delta and gamma (PPARα, PPARδ and PPARγ). Of these, PPARα was the most statistically significant ($p = 8.43\ E^{-19}$) upstream regulator and was predicted to be activated in BT2-treated mouse livers (Figure 7B). Similarly, the fatty acid beta oxidation pathway was one of the top 10 pathways significantly enriched in differentially expressed genes (-(log)p = 4.08) according to Ingenuity Canonical Pathway analysis (Figure 7C). To verify this gene signature, several known

PPARα target genes including *Cyp4a14* and *Acox1* were validated by quantitative RT-PCR in livers from fasted mice treated with vehicle or BT2, and each gene demonstrated increased expression in BT2-treated livers (Figure 7D). *Ppara* expression itself was also significantly transcriptionally upregulated in the RNAseq dataset (Supplemental Figure 5A). FGF-21, the expression of which was increased in BT2-treated animals (Figure 5O), is also a PPARα target [39]. To determine whether BT2 directly interacts with PPARα leading to its activation, an in vitro Lanthascreen assay was performed to assess PPARα activity. Known PPARα activator GW7647 demonstrated a dose-dependent increase in PPARα activity in this assay, whereas BT2 demonstrated no effect (Figure 7E). These data suggest that while BT2 treatment is activating PPARα target genes, the activation is likely physiological and not via a direct interaction of BT2 and PPARα.

3.7. Liver-specific knockdown of BDK does not improve metabolism or hepatic steatosis

It was previously demonstrated that adenovirus-mediated Ppm1k overexpression in Zucker fat rats improved metabolic homeostasis, and chronic BT2 treatment also improved hepatic steatosis [21]. These data suggested that hepatic BDK may have a cell autonomous role to drive metabolic homeostasis and hepatic steatosis, and conversely, that reduction of hepatic BDK may improve these parameters. To test this hypothesis, an AAV encoding *Bckdk* or scrambled shRNA was administered to age matched DIO mice (Figure 8A). Mice were maintained on HFD throughout the study duration, and body weights were unchanged by liver-specific BDK knockdown as compared with control AAV over an 8-week period (Figure 8B). After 8 weeks, an oGTT was performed, and no differences in glucose excursion or insulin levels were observed between the two groups (Figure 8C, D). Furthermore, liver weights were unchanged, and liver TG content was similar between control and BDK knockdown animals (Figure 8E, F). To confirm gene deletion, tissues were isolated, and quantitative RT-PCR was performed in liver, heart, and muscle. A significant 70% reduction of *Bckdk* was observed in livers from the mice treated with the AAV-sh(BCKDK) compared to the mice treated with AAV-sh(scramble), and a small reduction was also observed in heart while no change was noted in skeletal muscle (Figure 8G). *Gfp* mRNA was produced by both sh-Bckdk and scrambled AAV vectors, and similar expression was detected primarily in livers but was greatly reduced in heart (relative expression of approximately 3000) and largely absent in skeletal muscle (relative expression of approximately 500) (Figure 8H). At the protein level, there was also a significant 55% reduction of p-BCKDH and 75% reduction of BDK protein levels in the livers of the mice treated with AAV-sh(BCKDK) (Figure 8I). Terminal plasma BCAA and BCKA levels were assessed, and modest reductions in both BCAA (17%, 16%, 15% reductions for leucine, isoleucine and valine, respectively) and BCKA (25%, 25% and 11% for ketoleucine, ketoisoleucine and ketovaline, respectively) were observed in the AAV-sh(BCKDK) knockdown animal plasma (Figure 8J, K). Furthermore, quantitative RT-PCR assessment of PPARα target genes that were elevated by acute BT2 treatment remained unaltered or even reduced in BDK knockdown livers (Figure 8L). Thus, BDK knockdown was effective to reduce p-BCKDH and BDK protein levels in liver yet not effective to alter glucose homeostasis or liver steatosis, nor was liver-specific knockdown of BDK sufficient to activate PPARα target gene expression. These data suggest that while the effects of BDK inhibition rapidly affect metabolic endpoints such as insulin sensitivity and fasting-induced gene expression, these effects are likely mediated by a paracrine mechanism.

4. DISCUSSION

Defects in BCAA catabolism have long been associated with human inborn errors of metabolism and more recently with metabolic diseases such as T2D and NAFLD [1,2,12,14,15]. However, the mechanisms by which BCAA catabolism contributes to the pathogenesis of metabolic diseases remains elusive. Here, using BT2, an allosteric inhibitor of BDK [30], the contributions of BCAA catabolism, and the mechanisms by which this pathway contributes to metabolic disease and NAFLD were investigated. While previous reports had demonstrated improvements in glucose handling in mice that had been treated with BT2 chronically over several days or weeks [5,21], we demonstrate acute improvements in glucose handling (Figure 1) and insulin sensitivity (Figure 2). Remarkably, the effects of BDK inhibition on insulin sensitivity occurred in less than 1 h, indicating that the effect of increasing BCAA catabolism on metabolic parameters happens extremely rapidly.

The improvement in insulin sensitivity and metabolic health observed with BT2 treatment is similar to that observed with BCAA restricted diets, which has been assessed both in preclinical models and in humans [20,24,25]. BCAA restriction in rats was sufficient to increase fat oxidation in heart [19] and reduce the respiratory exchange ratio (RER) [24], which both support the notion that reducing BCAA levels is sufficient to drive fat oxidation. BT2 treatment also reduced RER in mice [21], and we have also observed reductions in RER upon BT2 treatment (unpublished observations). These rapid improvements in insulin sensitization and changes in fat oxidation may suggest that intracellular or metabolite signaling, rather than alterations in gene or protein expression, are mediating the effects observed. Indeed, a recent publication suggested that skeletal muscle BCKA overload resulting from lipotoxicity such as in metabolic syndrome can inhibit insulin sensitivity both in vitro and in vivo [40], and there was a significant reduction in BCKA levels in multiple tissue compartments including plasma, heart and muscle (Figure 1). In hyperinsulinemic hyperglycemic clamps, despite a significant increase in GIR, no significant changes were observed in any single component involved in glycemia control upon BT2 treatment, including hepatic glucose production, glucose disposal or muscle glucose uptake (Figure 2). This observation suggests that multiple tissues may be responsible for the improvement in insulin sensitivity upon increasing BCAA catabolism via BDK inhibition, perhaps by reducing systemic BCKA levels. A recent study suggested that metabolic benefits of BCAA restriction are mediated specifically by isoleucine and valine [41]. BT2 treatment reduces all BCAA and BCKA in mice by similar percentages (Figure 1), so it is challenging to speculate which BCAA may be most important in mediating the beneficial metabolic effects of BT2 treatment. BT2 treatment led to improvements in hepatic steatosis and/or inflammation in mice fed HFD (Figure 1), CDAHFD (Figure 3) and in *Ldlr*$^{-/-}$ mice fed Western diet (Figure 4). Each of these animal models have different mechanistic drivers [42], so it is interesting that BDK inhibition maintains its effects in all three conditions. In HFD-fed DIO mice, inflammation is a minimal component, and the steatosis observed is largely driven by de novo lipogenesis and/or impaired beta oxidation [42]. In CDAHFD, impaired lipid oxidation and VLDL production coupled with impaired VLDL export results in hepatic lipid accumulation [42]. Interestingly, in this model, AST and ALT levels were upregulated compared with vehicle after 4 weeks of BT2 treatment yet were reduced by 8 weeks of treatment (Figure 3E, F). This result may indicate that early in disease pathogenesis, BDK inhibition may not be protective in this model. These data suggest that BT2 may improve

hepatic steatosis at least in part by improving lipid oxidation or export, which is blocked by CDAHFD. However, as the disease progressed in this model, BDK inhibition with BT2 became protective (Figure 3). Finally, *Ldlr*$^{-/-}$ mice are hyperlipidemic and hypercholesterolemic, which when coupled with Western diet containing cholesterol leads to development of steatosis with mild to moderate inflammation and fibrosis [38,42]. It is tempting to consider that a common mechanism may be underlying this protection across the models, and RNAseq analyses of HFD-fed mouse livers after only 2 doses of BT2 identified increased expression of fatty acid oxidation gene expression and a PPARα activation signature as a possible common mechanistic link (Figure 7). Indeed, PPARα activation improves fatty acid oxidation and steatosis in several different animal models including those driven by methionine choline deficiency and hypercholesterolemia [43]. A recent study paradoxically demonstrated upregulation of PPARα transcription and fatty acid oxidation upon BCAA and BCKA treatment in cardiomyocytes even in the context of PP2Cm deletion, suggesting that BCAA or BCKA themselves, rather than a metabolite downstream of BCKDH were mediating this effect [44]. In our studies presented here, it is unclear how increasing BCAA catabolism leads to PPARα activation, as BT2 itself did not agonize PPARα in an in vitro system (Figure 7). We did observe small yet significant changes in PPARα transcript levels acutely in liver; however this level of induction is not likely to explain the effects that were observed (Supplemental Figure 5A). One hypothesis could be that BDK inhibition produces a factor that activates PPARα in a paracrine manner. PPARα is a nuclear receptor, and thus is activated by ligands derived from lipogenesis, lipolysis, and fatty acid catabolism [43]. Recent studies have identified that BCAA catabolism may produce branched chain fatty acids in adipose tissue [45]; it is possible that these ligands yet to be identified could have PPAR agonist activity.

It is remarkable that in a fasting and refeeding paradigm, BDK inhibition prevented many changes that occur with feeding, including hyperinsulinemia and suppression of ketogenesis. Moreover, acute treatment with BT2 completely prevented feeding-induced gene expression changes in liver (Figure 5). As BCAA are essential amino acids and must be obtained from dietary sources, this signature suggests that increasing BCAA catabolism and thus reducing BCAA levels may signal that the body is fasting. Interestingly, recent studies have suggested that BCAA may contribute to cardiac and skeletal myocyte hypertrophy in a circadian manner [46,47]. In these studies, consumption of high BCAAs at the beginning or the end of the awake period led to differing effects on myocyte hypertrophy [46,47]. Furthermore, the effects of BCAA consumption on myocyte hypertrophy were ameliorated in mice lacking Bmal, a component of the circadian clock [46,47]. Taken together, the studies presented herein support the hypothesis that BCAA serve as an anabolic signal, and BDK inhibition and therefore sustained systemic BCAA reductions may prolong the fasting-induced catabolic state to reduce postprandial hyperinsulinemia, prevent suppression of ketogenesis, and reduce lipid storage.

Despite the changes in insulin sensitivity, hepatic steatosis, and hepatic gene expression that were observed with BT2 treatment, AAV-mediated BDK knock down specifically in liver did not recapitulate any of these effects (Figure 8), suggesting that reducing BDK in liver is not sufficient to improve metabolism. Previous studies have demonstrated that adenoviral-mediated overexpression of the phosphatase Ppm1k, which dephosphorylates the same regulatory site on BCKDH as BDK phosphorylates, improved both glycemia and steatosis [21]. It is therefore surprising that while reducing pBCKDH by either inhibition of BDK with BT2 or overexpression of Ppm1k led to the same metabolic effects, BDK liver-specific knockdown did not. There are a few possibilities that could explain this finding. First, the knockdown of BDK in the liver, while efficient, was not complete. Second, previously reported Ppm1k overexpression studies utilized adenoviral delivery, which may have caused Ppm1k expression in additional tissues such as spleen [48]. Third, species differences in BDK gene regulation have been reported [21], so BDK knockdown in mouse may not have the same effect as it would have in a different species such as rat. Future studies will be needed to investigate these possibilities.

One question that remains outstanding is whether there is a key tissue that is driving the improvement in metabolism in response to BT2 treatment. While recent studies have suggested a critical role for adipocytes and adipose tissue in BCAA homeostasis [49,50], here we do not observe changes in body weight, nor are morphological differences observed in WAT after chronic BT2 treatment (Supplemental Figure 1). pBCKDH was also not significantly reduced in WAT with acute BT2 treatment (Figure 5). Furthermore, while the BCAA/BCKA axis is reportedly important for thermogenesis and AT browning in mice, pBCKDH was not significantly reduced in WAT or BAT after acute BT2 treatment. BT2 is an acidic compound so biodistribution of the compound could be poor in adipose tissue [51], which could suggest that the role of adipose tissue in BT2-mediated metabolic effects is not as profound as a genetic knockout in this tissue. Additionally, all of the studies reported here were performed at room temperature, so differences may have been observed in metabolism after BT2 treatment during cold challenge or in thermoneutrality. It would be interesting to investigate those conditions in future studies. Similarly, the central effects of BT2 treatment were not investigated here. We have found in pharmacokinetic studies that BT2 is a brain impaired compound with a brain:plasma biodistribution ratio of 0.007 (10 mpk SC 24 h plasma AUC 375000 ng*hr/ml, brain AUC 2670 ng*hr/ml), so BT2 is unlikely to have any direct central effects. However, we cannot preclude an indirect effect of BCAA lowering on brain chemistry in our studies. Taken together, results from the current series of studies suggest that the beneficial effects of BT2 inhibition on whole body metabolism is likely derived from systemic inhibition of BDK and the resulting modulation of BCAA catabolism that requires the involvement of multiple tissues.

There are multiple limitations of this study. First, chow mice were not included in the 13C glucose infusion studies conducted in Figure 2, which would have been important to understand suppression of hepatic glucose output. Next, only male mice were used in this manuscript, so it is possible that different physiological phenotypes could have been observed if female mice had been used. Finally, it would have been informative to assess correlation between BCAA/BCKA lowering and efficacy phenotypes including glucose homeostasis (Figure 1) insulin sensitivity (Figure 2) liver steatosis (Figures 3 and 4), and gene expression (Figures 5 and 7). BCAA/BCKA lowering is time and dose-dependent, and the reduction in BCAA/BCKA is maximal approximately 30 min post administration of BT2 (Figure 1). Within this manuscript, most animals were euthanized 1 h post final dose of compound, at C_{max}. Therefore, it is challenging to define strict dose—response relationships, as the efficacy endpoints measured here are likely a reflection of the 24 h average concentrations of BCAA/BCKA rather than the maximal reduction measured 1 h post dose.

In summary, in addition to confirming previous reports that BDK inhibition with BT2 improves glycemia and NAFLD, we have expanded upon mechanistic understanding of how BDK inhibition improves metabolism. BT2 treatment improved insulin sensitivity and glucose tolerance extremely rapidly and improved hepatic steatosis and/or inflammation in several mouse models of NAFLD and NASH. Fasting

and refeeding studies suggested that BT2 treatment prolonged the fasting response at both a hormonal and transcriptional level and increased the expression of genes related to fatty acid oxidation. However, these effects were not mediated by a cell autonomous effect of BDK within the liver. Taken together, these data suggest that BDK inhibition may alter systemic metabolism to promote paracrine tissue cross talk to improve metabolism. Therefore, BDK inhibition may be an effective therapeutic to improve multiple facets of metabolic syndrome.

AUTHOR CONTRIBUTIONS

RJRF, RAM, BBZ, EB, KJF, AH, MC, CS designed research, EB, MP, JL, BA, TG, AS, ZS, GX, BT, SG, CPS, SRV, AR, LCG, MM, GW, RJRF performed research, EB, EP, MC, JCS, FG, RAM, RJRF analyzed data, and RJRF & EB wrote the manuscript.

FUNDING SOURCES

All studies were funded by Pfizer, Inc.

DATA AVAILABILITY

Data will be made available on request.

ACKNOWLEDGEMENTS

The authors would like to acknowledge Donald Bennett, Timothy Coskran, Collin Crowley, Natalie Daurio Ochocki, Ghazal Hariri, Lina Luo, Shawn O'Neil, Gary Seitis, Abdul Sheikh, LouJin Song, Ka Ning Yip, Heather Eng, Jie Chen, Amit Kalgutkar, Sheila Kantesaria, Greg Tesz, and Chang Zou for technical assistance.

CONFLICT OF INTEREST

All authors are employees of Pfizer Inc. or were employees at the time the research was conducted.

APPENDIX A. SUPPLEMENTARY DATA

Supplementary data to this article can be found online at https://doi.org/10.1016/j.molmet.2022.101611.

REFERENCES

[1] Newgard, C.B., An, J., Bain, J.R., Muehlbauer, M.J., Stevens, R.D., Lien, L.F., et al., 2009. A branched-chain amino acid-related metabolic signature that differentiates obese and lean humans and contributes to insulin resistance. Cell Metabolism 9(4):311–326.

[2] Wang, T.J., Larson, M.G., Vasan, R.S., Cheng, S., Rhee, E.P., McCabe, E., et al., 2011. Metabolite profiles and the risk of developing diabetes. Nature Medicine 17(4):448–453.

[3] Lotta, L.A., Scott, R.A., Sharp, S.J., Burgess, S., Luan, J., Tillin, T., et al., 2016. Genetic predisposition to an impaired metabolism of the branched-chain amino acids and risk of type 2 diabetes: a mendelian randomisation analysis. PLoS Medicine 13(11):e1002179.

[4] Menni, C., Fauman, E., Erte, I., Perry, J.R., Kastenmuller, G., Shin, S.Y., et al., 2013. Biomarkers for type 2 diabetes and impaired fasting glucose using a nontargeted metabolomics approach. Diabetes 62(12):4270–4276.

[5] Zhou, M., Shao, J., Wu, C.Y., Shu, L., Dong, W., Liu, Y., et al., 2019. Targeting BCAA catabolism to treat obesity-associated insulin resistance. Diabetes 68(9):1730–1746.

[6] Mardinoglu, A., Gogg, S., Lotta, L.A., Stancakova, A., Nerstedt, A., Boren, J., et al., 2018. Elevated plasma levels of 3-hydroxyisobutyric acid are associated with incident type 2 diabetes. EBioMedicine 27:151–155.

[7] Lai, L., Leone, T.C., Keller, M.P., Martin, O.J., Broman, A.T., Nigro, J., et al., 2014. Energy metabolic reprogramming in the hypertrophied and early stage failing heart: a multisystems approach. Circulation: Heart Failure 7(6):1022–1031.

[8] Sun, H., Olson, K.C., Gao, C., Prosdocimo, D.A., Zhou, M., Wang, Z., et al., 2016. Catabolic defect of branched-chain amino acids promotes heart failure. Circulation 133(21):2038–2049.

[9] Uddin, G.M., Zhang, L., Shah, S., Fukushima, A., Wagg, C.S., Gopal, K., et al., 2019. Impaired branched chain amino acid oxidation contributes to cardiac insulin resistance in heart failure. Cardiovascular Diabetology 18(1):86.

[10] Wang, W., Zhang, F., Xia, Y., Zhao, S., Yan, W., Wang, H., et al., 2016. Defective branched chain amino acid catabolism contributes to cardiac dysfunction and remodeling following myocardial infarction. American Journal of Physiology - Heart and Circulatory Physiology 311(5):H1160–H1169.

[11] Li, T., Zhang, Z., Kolwicz Jr., S.C., Abell, L., Roe, N.D., Kim, M., et al., 2017. Defective branched-chain amino acid catabolism disrupts glucose metabolism and sensitizes the heart to ischemia-reperfusion injury. Cell Metabolism 25(2):374–385.

[12] Lake, A.D., Novak, P., Shipkova, P., Aranibar, N., Robertson, D.G., Reily, M.D., et al., 2015. Branched chain amino acid metabolism profiles in progressive human nonalcoholic fatty liver disease. Amino Acids 47(3):603–615.

[13] Biswas, D., Tozer, K., Dao, K.T., Perez, L.J., Mercer, A., Brown, A., et al., 2020. Adverse outcomes in obese cardiac surgery patients correlates with altered branched-chain amino acid catabolism in adipose tissue and heart. Frontiers in Endocrinology (Lausanne) 11:534.

[14] Neinast, M., Murashige, D., Arany, Z., 2019. Branched chain amino acids. Annual Review of Physiology 81:139–164.

[15] Lynch, C.J., Adams, S.H., 2014. Branched-chain amino acids in metabolic signalling and insulin resistance. Nature Reviews Endocrinology 10(12):723–736.

[16] Biswas, D., Duffley, L., Pulinilkunnil, T., 2019. Role of branched-chain amino acid-catabolizing enzymes in intertissue signaling, metabolic remodeling, and energy homeostasis. The FASEB Journal 33(8):8711–8731.

[17] Lu, G., Sun, H., She, P., Youn, J.Y., Warburton, S., Ping, P., et al., 2009. Protein phosphatase 2Cm is a critical regulator of branched-chain amino acid catabolism in mice and cultured cells. Journal of Clinical Investigation 119(6):1678–1687.

[18] East, M.P., Laitinen, T., Asquith, C.R.M., 2021. BCKDK: an emerging kinase target for metabolic diseases and cancer. Nature Reviews Drug Discovery 20(7):498.

[19] McGarrah, R.W., Zhang, G.F., Christopher, B.A., Deleye, Y., Walejko, J.M., Page, S., et al., 2020. Dietary branched-chain amino acid restriction alters fuel selection and reduces triglyceride stores in hearts of Zucker fatty rats. American Journal of Physiology. Endocrinology and Metabolism 318(2):E216–E223.

[20] Fontana, L., Cummings, N.E., Arriola Apelo, S.I., Neuman, J.C., Kasza, I., Schmidt, B.A., et al., 2016. Decreased consumption of branched-chain amino acids improves metabolic health. Cell Reports 16(2):520–530.

[21] White, P.J., McGarrah, R.W., Grimsrud, P.A., Tso, S.C., Yang, W.H., Haldeman, J.M., et al., 2018. The BCKDH kinase and phosphatase integrate BCAA and lipid metabolism via regulation of ATP-citrate lyase. Cell Metabolism 27(6):1281–1293 e1287.

[22] She, P., Reid, T.M., Bronson, S.K., Vary, T.C., Hajnal, A., Lynch, C.J., et al., 2007. Disruption of BCATm in mice leads to increased energy expenditure associated with the activation of a futile protein turnover cycle. Cell Metabolism 6(3):181–194.

[23] Karusheva, Y., Koessler, T., Strassburger, K., Markgraf, D., Mastrototaro, L., Jelenik, T., et al., 2019. Short-term dietary reduction of branched-chain amino

acids reduces meal-induced insulin secretion and modifies microbiome composition in type 2 diabetes: a randomized controlled crossover trial. American Journal of Clinical Nutrition 110(5):1098—1107.

[24] White, P.J., Lapworth, A.L., An, J., Wang, L., McGarrah, R.W., Stevens, R.D., et al., 2016. Branched-chain amino acid restriction in Zucker-fatty rats improves muscle insulin sensitivity by enhancing efficiency of fatty acid oxidation and acyl-glycine export. Molecular Metabolism 5(7):538—551.

[25] Cummings, N.E., Williams, E.M., Kasza, I., Konon, E.N., Schaid, M.D., Schmidt, B.A., et al., 2018. Restoration of metabolic health by decreased consumption of branched-chain amino acids. Journal of Physiology 596(4): 623—645.

[26] Wang, J., Liu, Y., Lian, K., Shentu, X., Fang, J., Shao, J., et al., 2019. BCAA catabolic defect alters glucose metabolism in lean mice. Frontiers in Physiology 10:1140.

[27] Zigler Jr., J.S., Hodgkinson, C.A., Wright, M., Klise, A., Sundin, O., Broman, K.W., et al., 2016. A spontaneous missense mutation in branched chain keto acid dehydrogenase kinase in the rat affects both the central and peripheral nervous systems. PLoS One 11(7):e0160447.

[28] Joshi, M.A., Jeoung, N.H., Obayashi, M., Hattab, E.M., Brocken, E.G., Liechty, E.A., et al., 2006. Impaired growth and neurological abnormalities in branched-chain alpha-keto acid dehydrogenase kinase-deficient mice. Biochemical Journal 400(1):153—162.

[29] Tso, S.C., Qi, X., Gui, W.J., Chuang, J.L., Morlock, L.K., Wallace, A.L., et al., 2013. Structure-based design and mechanisms of allosteric inhibitors for mitochondrial branched-chain alpha-ketoacid dehydrogenase kinase. Proceedings of the National Academy of Sciences of the U S A 110(24):9728—9733.

[30] Tso, S.C., Gui, W.J., Wu, C.Y., Chuang, J.L., Qi, X., Skvora, K.J., et al., 2014. Benzothiophene carboxylate derivatives as novel allosteric inhibitors of branched-chain alpha-ketoacid dehydrogenase kinase. Journal of Biological Chemistry 289(30):20583—20593.

[31] Neinast, M.D., Jang, C., Hui, S., Murashige, D.S., Chu, Q., Morscher, R.J., et al., 2019. Quantitative analysis of the whole-body metabolic fate of branched-chain amino acids. Cell Metabolism 29(2):417—429 e414.

[32] Zhao, S., Xi, L., Quan, J., Xi, H., Zhang, Y., von Schack, D., et al., 2016. QuickRNASeq lifts large-scale RNA-seq data analyses to the next level of automation and interactive visualization. BMC Genomics 17:39.

[33] Love, M.I., Huber, W., Anders, S., 2014. Moderated estimation of fold change and dispersion for RNA-seq data with DESeq2. Genome Biology 15(12):550.

[34] Kramer, A., Green, J., Pollard Jr., J., Tugendreich, S., 2014. Causal analysis approaches in ingenuity pathway analysis. Bioinformatics 30(4):523—530.

[35] Longo, V.D., Anderson, R.M., 2022. Nutrition, longevity and disease: from molecular mechanisms to interventions. Cell 185(9):1455—1470.

[36] Gaggini, M., Carli, F., Rosso, C., Buzzigoli, E., Marietti, M., Della Latta, V., et al., 2018. Altered amino acid concentrations in NAFLD: impact of obesity and insulin resistance. Hepatology 67(1):145—158.

[37] Matsumoto, M., Hada, N., Sakamaki, Y., Uno, A., Shiga, T., Tanaka, C., et al., 2013. An improved mouse model that rapidly develops fibrosis in non-alcoholic steatohepatitis. International Journal of Experimental Pathology 94(2):93—103.

[38] Bieghs, V., Van Gorp, P.J., Wouters, K., Hendrikx, T., Gijbels, M.J., van Bilsen, M., et al., 2012. LDL receptor knock-out mice are a physiological model particularly vulnerable to study the onset of inflammation in non-alcoholic fatty liver disease. PLoS One 7(1):e30668.

[39] Badman, M.K., Pissios, P., Kennedy, A.R., Koukos, G., Flier, J.S., Maratos-Flier, E., 2007. Hepatic fibroblast growth factor 21 is regulated by PPARalpha and is a key mediator of hepatic lipid metabolism in ketotic states. Cell Metabolism 5(6):426—437.

[40] Biswas, D., Dao, K.T., Mercer, A., Cowie, A.M., Duffley, L., El Hiani, Y., et al., 2020. Branched-chain ketoacid overload inhibits insulin action in the muscle. Journal of Biological Chemistry 295(46):15597—15621.

[41] Yu, D., Richardson, N.E., Green, C.L., Spicer, A.B., Murphy, M.E., Flores, V., et al., 2021. The adverse metabolic effects of branched-chain amino acids are mediated by isoleucine and valine. Cell Metabolism 33(5):905—922 e906.

[42] Van Herck, M.A., Vonghia, L., Francque, S.M., 2017. Animal models of nonalcoholic fatty liver disease-A starter's guide. Nutrients 9(10).

[43] Pawlak, M., Lefebvre, P., Staels, B., 2015. Molecular mechanism of PPAR-alpha action and its impact on lipid metabolism, inflammation and fibrosis in non-alcoholic fatty liver disease. Journal of Hepatology 62(3):720—733.

[44] Li, Y., Xiong, Z., Yan, W., Gao, E., Cheng, H., Wu, G., et al., 2020. Branched chain amino acids exacerbate myocardial ischemia/reperfusion vulnerability via enhancing GCN2/ATF6/PPAR-alpha pathway-dependent fatty acid oxidation. Theranostics 10(12):5623—5640.

[45] Wallace, M., Green, C.R., Roberts, L.S., Lee, Y.M., McCarville, J.L., Sanchez-Gurmaches, J., et al., 2018. Enzyme promiscuity drives branched-chain fatty acid synthesis in adipose tissues. Nature Chemical Biology 14(11):1021—1031.

[46] Latimer, M.N., Sonkar, R., Mia, S., Frayne, I.R., Carter, K.J., Johnson, C.A., et al., 2021. Branched chain amino acids selectively promote cardiac growth at the end of the awake period. Journal of Molecular and Cellular Cardiology 157:31—44.

[47] Aoyama, S., Kim, H.K., Hirooka, R., Tanaka, M., Shimoda, T., Chijiki, H., et al., 2021. Distribution of dietary protein intake in daily meals influences skeletal muscle hypertrophy via the muscle clock. Cell Reports 36(1):109336.

[48] Kamimura, K., Suda, T., Zhang, G., Liu, D., 2011. Advances in gene delivery systems. Pharmaceutical Medicine 25(5):293—306.

[49] Yoneshiro, T., Wang, Q., Tajima, K., Matsushita, M., Maki, H., Igarashi, K., et al., 2019. BCAA catabolism in brown fat controls energy homeostasis through SLC25A44. Nature 572(7771):614—619.

[50] Ma, Q.X., Zhu, W.Y., Lu, X.C., Jiang, D., Xu, F., Li, J.T., et al., 2022. BCAA-BCKA axis regulates WAT browning through acetylation of PRDM16. Nature Metabolism 4(1):106—122.

[51] Orozco, C.C., Atkinson, K., Ryu, S., Chang, G., Keefer, C., Lin, J., et al., 2020. Structural attributes influencing unbound tissue distribution. European Journal of Medicinal Chemistry 185:111813.

